Bachelor's Thesis

Bachelor's degree in Industrial Technology Engineering

Modelling, Control and Simulation of a Microgrid based on PV System, Battery System and VSC

REPORT

Author: Silvia Ma Lu
Director: Oriol Gomis Bellmunt
Announcement: January 2018

Escola Tècnica Superior
d'Enginyeria Industrial de Barcelona

Abstract

Nowadays, where the renewable energies are the new trend and sustainable technologies are starting to play a big role in the society in order to eliminate the dependence on fossil fuels, finding the way to collect these clean energies and to convert them into electricity at their highest performance is without any doubt essential. Nevertheless, the way to link the power generated from these renewable sources to the main grid is as well significant.

The present project studies step by step the design, modelling, control and simulation of a microgrid based on several elements with a special focus to the Photovoltaic (PV) System and to the Voltage Source Converters (VSC).

Modelling of the equivalent electric circuit model to simulate the working principle of a PV cell is studied in detail and a Maximum Power Point Tracking (MPPT) control algorithm to force the PV system works at its highest operation point is applied.

A complete review of the two level VSC simplified model is elaborated and implemented to connect two DC sources (PV system and Battery system) to the main AC three-phase grid. Additionally, examples using the two level VSC real model based on six Insulated Gate Bipolar Transistors (IGBT) are tested, where the voltages modulation are obtained by applying Sinusoidal Pulse Width Modulation (SPWM).

The control methodology for the several elements of the microgrid, most of them based on Proportional – Integral (PI) controllers to reduce the steady-state error to zero, ensures that a change in an input parameter of the system alters other components in order to reach a new balanced state in a small amount of time. The operation and behaviour of the entire microgrid is checked using software MATLAB Simulink and the results show a proper performance.

Table of contents

Table of figures

Table of tables

1. Glossary of terms

AC	Alternating Current
CSP	Concentrated Solar Power
DC	Direct Current
DSSC	Dye Sensitized Solar Cell
EPIA	European Photovoltaic Industry Association
IEA	International Energy Agency
IGBT	Insulated Gate Bipolar Transistor
IV	Current – Voltage
LCC	Line Commutated Converter
MPP	Maximum Power Point
MPPT	Maximum Power Point Tracking
PI	Proportional – Integral
PLL	Phase Locked Loop
PV	Photovoltaic
PVPS	Photovoltaic Power Systems
PWM	Pulse Width Modulation
SPWM	Sinusoidal Pulse Width Modulation
VSC	Voltage Source Converter

2. Preface

2.1. Project origin

The present project has emerged due to the great interest of the author to the world of renewable energies, especially to solar energy. First contact with this field could be tracked down to the summer when the author finished Secondary school, the author could develop a project on Solar Energy about Dye Sensitized Solar Cells (DSSC), a type of solar cell based on natural dyes to generate power and it was possible thanks to Catalunya Caixa Foundation.

From then, the author was able to deepen about the several methods to obtain electrical or thermal power from Sun's energy during the degree although there was not any specific course about the topic. For instance, for Project Management course, a study to integrate thermal solar energy for sanitary hot water to a building was elaborated.

Nevertheless, solar energy is not only about the different technologies to gather the Sun's energy and to convert it into electricity or thermal energy at the maximum efficiency, it is also overriding the way to introduce this collected energy to the main grid. In fact, the distribution of the energy obtained from solar energy to the grid was a complete unknown topic for the author. Hence, among the topics listed for possible thesis projects, there was the Electrical Engineering Department offering thesis projects related to it. This project has helped the author to enhance knowledge on photovoltaic solar energy, converters and grid connected systems.

2.2. Previous knowledge requirements

In order to enter to the world of electrical grids and photovoltaic cell on its most electrical adaptation, notions of electrical engineering for understanding and computing power balances, basic electronics to comprehend the components of a converter or the electrical model of a photovoltaic cell, and system dynamics to design the controllers are required.

3. Introduction

One of the main topics that the world faces nowadays is the need to become less dependent on fossil fuels, a problem that can be minimized with the help of renewable energies. It is expected that renewable energies will substitute the fossil fuels not only because they are cleaner (less CO_2 emissions) but they are also inexhaustible. Finding the way to increase the efficiency of these clean energies is vital, however, a proper connection between the renewable generation source and the main grid is also indispensable.

Hence, the present project aims to design, to model, to control and to simulate a small scale distributed generation system based on a renewable generation source and a storage generation system altogether with a load and the main power grid. In fact, the previous description is a close definition of a microgrid [1].

The structure of the project starts with defining the goals and scope in the current chapter 3. Then, in chapter 4, basic knowledge about the chosen renewable energy source and inverters are explained. Next chapter, 5, the components of the studied system are described. Chapter 6 deals with the modelling of all the elements that form the studied microgrid. Chapter 7 explains the control of the previously modelled elements. The following chapter 8 contains the simulations carried out and the analysis of the results. Chapter 9 and 10 collect the economic study and the environmental impact of the project respectively. Finally, last chapter 11, conclusions extracted from the present project are summarized.

3.1. Project objectives

The main target of this project is to model a microgrid, to later simulate the performance of it and verify that the behaviour and consequently the modelling are correct. For this reason, sub goals could be defined as:

- Analysis, modelling and control study of the Voltage Source Converters (VSC) due to they will be the kind of inverters applied.
- Design, modelling and control study of the solar photovoltaic (PV) cell due to this will be the renewable energy technology implemented.
- Simple design, modelling and control of secondary elements of the microgrid in reference to the energy storage system (based on a battery) and the load.

3.2. Scope of the project

The scope includes the modelling and control study of the VSC, the design, modelling and control of a PV system with a Maximum Power Point Tracking (MPPT) algorithm, a simplified modelling of a battery system and a constant load. The energy management system is not contemplated although it exists. It also includes the performance analysis of the mentioned elements connected to create the microgrid. All the results from the simulations are carried out using software tool Matlab Simulink.

Additionally, simulations using the real model of the VSC (due to for the modelling of the entire microgrid they have been modelled ideally) are performed for two scenarios: storage system connected to the grid and renewable generation system connected to the grid. Both connections from DC source to AC grid are made by means of real model VSC (i.e, using IGBT) and Sinusoidal Pulse Width Modulation (SPWM) technique is applied to modulate the voltages.

4. Basic and generalities of Solar Photovoltaic Energy

The present chapter aims to inform the lector about the current situation of Solar Energy production, to give some basic knowledge about the working principle of solar photovoltaic and also about inverters in order to understand the following chapters with ease.

4.1. Present situation of Solar Photovoltaic production

Nowadays, there are two big types of solar power production. One of them is Solar Photovoltaic (PV) Systems, which uses solar panels to convert sunlight directly into electric power. The other one is Concentrated Solar Power (CSP) also known as "concentrated solar thermal", this method uses solar thermal energy to make steam that is converted into electricity by a turbine thereafter.

During the last years, the growth of photovoltaic has been very strong worldwide. With the aim of moving towards a low carbon economy, each country has its target and even the European Commission has its own, for example, the Renewable Energy Directive sets rules for the EU to achieve its 20% renewables target by 2020 [2]. In 2015, global Solar PV capacity achieved 227 GW while CSP capacity reached 4,80 GW among 785 GW of total renewable power capacity (not including hydro) [3]. By the end of 2016, installed global photovoltaic capacity increased to at least 303 GW, which equals to 1,80 % of the electricity demand of the planet. The covered demand percentage might seem low, however, back in 2000 the total amount of PV installed was only 170 MW, compared to now the growth is considerable [4]. Top countries installing PV system during the last years are observed in Figure 4.1.

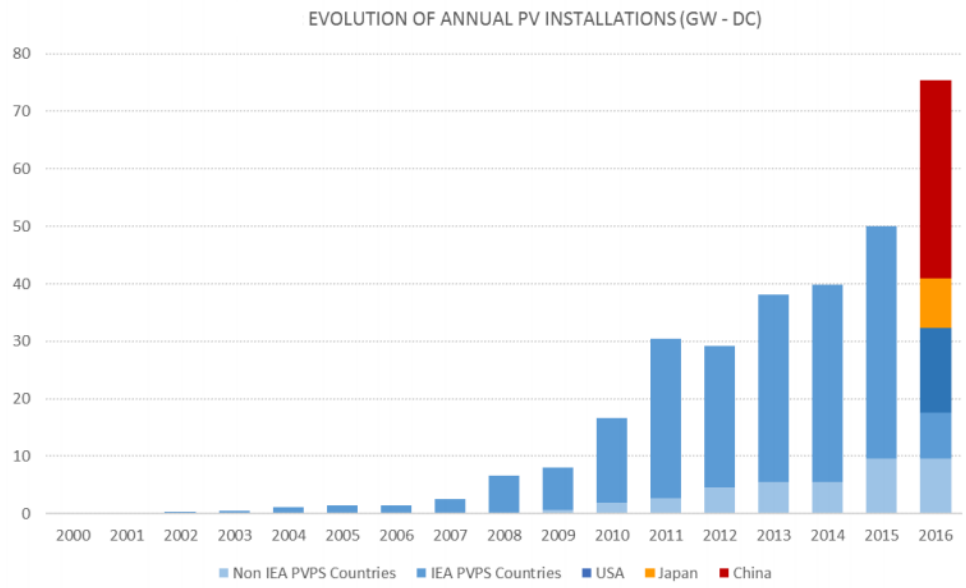

Figure 4.1 Evolution of annual PV installations from top countries. Source: [4]

4.1.1. Spain Solar PV production

Even though Spain has one of the highest levels of solar irradiance in Europe, its growth has slowed down significantly compared to the rest of Europe. In 2011 the total installed solar capacity was 4,89 GW and in 2016 the value just increased to 5,50 GW [5]. It is true that the Spain's national target for solar capacity by 2020 is easily reachable (8,37 GW) although the EPIA (European Photovoltaic Industry Association) estimates that Spain should be able to add over 1500 MW of solar energy every year [6]. The main reason of the decrease in growth is due to the end of subsidies to solar energy in 2012 as a result of a wider economic review by the Spanish government [6]. Moreover, in October 2015, Spain's Council of Ministers approved a 'sun tax' on those using electricity produced by their own solar installation.

This legislation says that those with self-consumptive photovoltaic systems have to pay the same grid fees as those without solar panels (assuming they are still connected to the grid), besides, they have to pay a second 'sun tax' for the electricity they generate and use from their PV systems, even though it does not come into contact with the grid. Likewise, the new law says that PV systems up to 100 kW are not able to sell any excess of electricity they produce. Instead, they must donate the extra electricity to the grid for free. Following the same line, this legislation has a few more laws discouraging people to install PV eco-friendly systems [7].

Nevertheless, this legislation will probably come to an end soon and from then, Spain will be able to impulse its production again and to take advantage of the favourable location that it has to produce solar energy.

4.2. Working Principle of Solar PV

The following section will explain how a solar cell works and how is its equivalent circuit model.

4.2.1. Solar Cell Structure

A solar cell is an electronic device which directly converts sunlight into electricity. The mechanism in which solar light is directly converted into voltage or current is called the photovoltaic effect. Basic steps in the operation of a solar cell are:

a. The generation of light generated carriers (electrons and holes): due to the absorption of incident photons by the material (semiconductor, typically silicon: Si) to create electron-hole pairs provided that the incident photon has an energy greater than that of the band gap.
b. The collection of the light-generated carriers by the p-n junction to generate a current: due to the existing electric field at the p-n junction, the p-n junction spatially separates the electron (to the n-type zone) and the hole (to the p-type zone) to prevent its recombination.

c. The collection of the charge carriers at the contacts and the generation of a large voltage across the solar cell.
d. The dissipation of power in the load and in parasitic resistances.

A representation scheme of the solar cell operation can be observed in Figure 4.2.

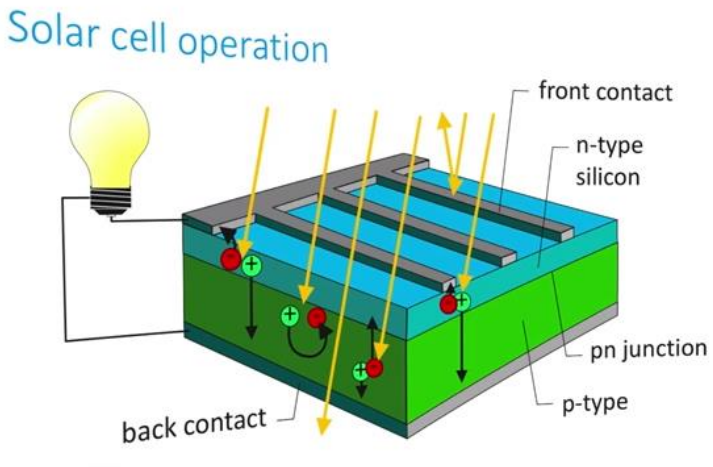

Figure 4.2 Simplified representation of a silicon based solar cell and its operation. Source: [8]

4.2.2. Equivalent circuit model

The performance of a solar cell can be demonstrated by measuring its current versus the voltage (IV curve –Figure 4.3). The IV curve is the superposition of the IV curve of the solar cell diode in the dark with the light-generated current.

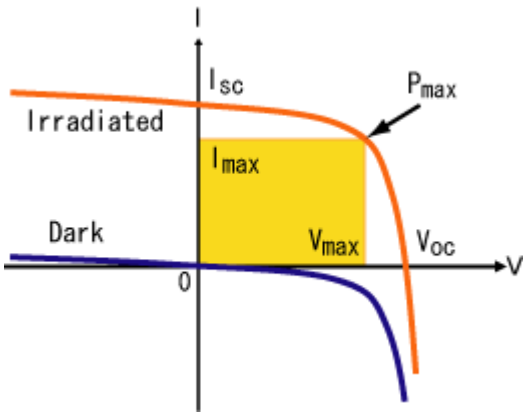

Figure 4.3 Common IV curve from a solar cell. Source: [9]

In the dark, the IV curve of a solar cell has an exponential characteristic similar to that of a diode under no illumination (equation (4.1), parameters are described in section 6.1).

$$I_D = I_{dark} = I_0 exp\left(\frac{qV}{k_B T}\right) \quad (4.1)$$

The solar cell will block current under reverse bias conditions and it will produce current under forward bias conditions.

Under illumination, the solar cell conducts additional current related to the light excited charge carriers and thus, the IV curve shifts as the cell begins to generate power.

This behaviour can be described as an electrical circuit, in Figure 4.4 an equivalent model of an ideal solar cell is represented. The photo generated current is represented by a current source (I_{PH}) and the diode of the solar cell in the dark is represented by the triangle shape symbol (I_D).

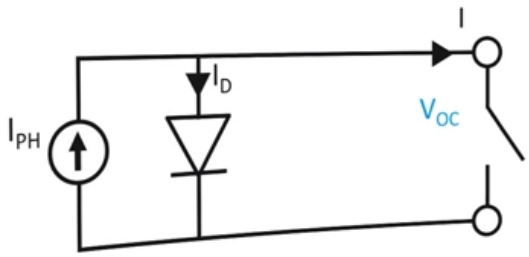

Figure 4.4 Equivalent electrical circuit model of an ideal solar cell under open circuit voltage situation. Source: [8]

When it is open circuited (Figure 4.4), nothing is connected to the cell and it is only producing voltage and no current, the voltage is called open circuit voltage. When the external circuit of the cell is connected in a short circuit without any external resistance, the solar cell is only producing current a no voltage thus the current that is running through the device is called the short circuit current (Figure 4.5).

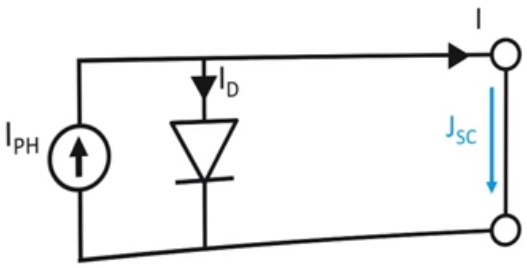

Figure 4.5 Equivalent electrical circuit model of an ideal solar cell under short circuit current situation. Source: [8]

Both parameters, V_{OC} and I_{SC}, define the IV curve. The power of a solar cell is defined as the voltage multiplied by the current at any point on the IV curve. With the IV curve it is possible to determine the maximum power point (MPP). In Figure 4.6 it is represented the power versus the current (red line). The current and voltage where the maximum power point is located are also two parameters that define the characteristics of the solar module. That power is the one delivered to the rest of the PV system and eventually to the load. Therefore, it is essential that the solar module

operates at the maximum power (further information see section 7.1).

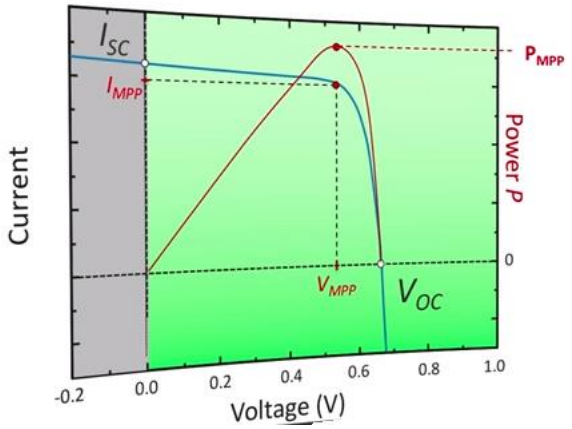

Figure 4.6 IV Curve and PC curve of a solar cell. Source: [8]

A more accurate electrical circuit of a solar cell is the one represented in Figure 4.7 with the parasitic resistances and it is the one to take consideration of when modelling. The equation for the electrical circuit applying Kirchhoff's laws is equation (4.2) and an elaborated version is expressed in equation (4.3) explained later in section 6.1.

$$I = I_L - I_D - I' \tag{4.2}$$

$$I = I_L - I_0 \exp\left[\frac{q(V+IR_S)}{nkT}\right] - \frac{V+IR_S}{R_{SH}} \tag{4.3}$$

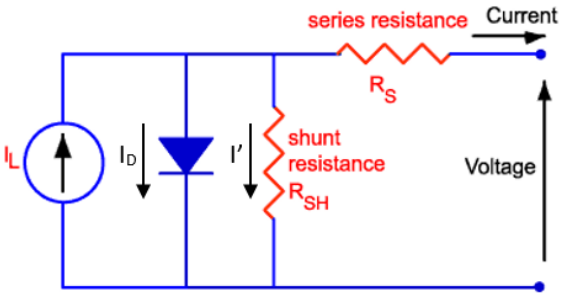

Figure 4.7 Equivalent circuit of a non-ideal solar cell.
Source: [10]

4.2.2.1. Effect of the parasitic resistances

Resistive effects in solar cells reduce the efficiency of the solar cells by dissipating power in the resistances. Most common parasitic resistances are series resistance and shunt resistance. Both magnitude and impact of the Rs and Rsh depend on the geometry of the solar cell at the operating point [10].

4.2.2.1.1 Series resistances

Series resistances in a solar cell has mainly three causes: the movement of current through the emitter and the base of the solar cell, the contact resistance between the metal contact and the silicon, and the resistance of the top and rear metal contacts.

4.2.2.1.2 Shunt resistances

Significant power losses caused by the presence of a shunt resistance are typically due to manufacturing defects rather than poor solar cell design.

4.3. Typology of Power converters

A photovoltaic (PV) system to be widely usable needs a solar inverter, one of the most important power electronic devices. It makes the DC power from the modules usable for all the appliances in a house. Although these appliances might internally either work with DC or AC, all of them are used to an AC grid. DC is produced by power sources like batteries, laptop chargers or solar cells. AC power is chosen as the standard for central power generation, transmission and distribution. In short words, the inverter converts a DC electric signal into an AC one.

A wide variety of converter typologies exists and they are classified based on their mode of operation, implementation topology or the kind of semiconductor used.

4.3.1. Mode of operation typologies

- Grid-connected systems: the load can be supplied either by the PV system or the grid depending on the available irradiance and the demand (Figure 4.8). The inverter latches on to the grid's frequency and voltage. Therefore, the inverter that supplies AC power to the grid acts as a current source, while the role of the constant voltage source in the system is fulfilled by the grid.

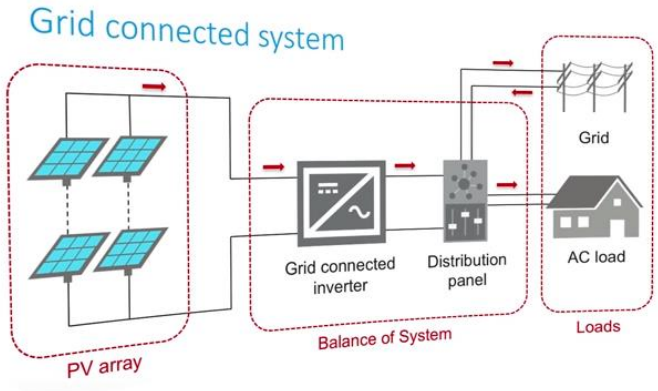

Figure 4.8 Grid connected system scheme. Source: [11]

- Stand-alone systems: there is no grid availability (Figure 4.9). The excess of energy produced has to be stored in order for the system to still be able to operate, even at

night, when there is no PV power generation. The load can only depend on the PV system for power, thus, the inverter that supplies AC power to the load has to appear as a voltage source with a stable voltage and frequency.

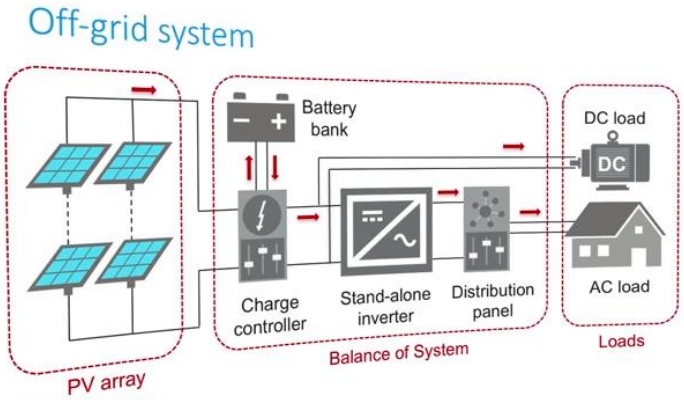

Figure 4.9 Stand-alone system scheme. Source: [11]

- Bimodal inverters: applied in situations that require both connection types.

4.3.2. Implementation topologies

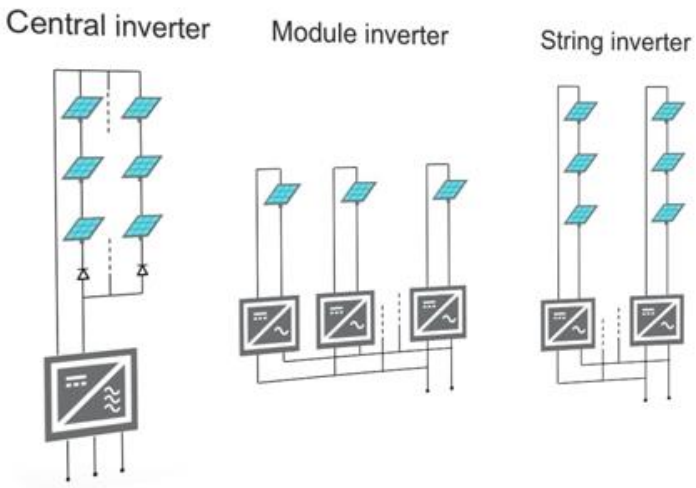

Figure 4.10 Implementation topologies of inverters.
Source [11]

Main implementation topologies are represented in Figure 4.10.

- Central inverter: most traditional in use. One central inverter catering to all PV modules in a PV system.
- Module inverter (microinverters): each module has a dedicated inverter with an MPP tracker.
- String inverter: PV modules connected in series. More resilient to mismatch than central inverter because each string is independently operated at its MPP.

The choice of an inverter based on the implementation topology will depend on the system needs, size and budget.

4.3.3. Kind of semiconductor

Regarding to the kind of semiconductor used, inverters can be classified on [12]:

- Inverters based on Insulated Gate Bipolar Transistor (IGBT): they provide fast switching and it is possible to modulate any desired voltage. The resulting converters are the Voltage Source Converters (VSC) which are able to control independently active and reactive power and inject reduced harmonic currents allowing to use lighter filters. However, a higher switching frequency means higher losses.
- Inverters based on thyristor: they require the grid to be operated and large filters for the important harmonic currents they generate. The resulting converters are called Line Commutated Converters (LCC), they are able to control active power while consuming non controllable reactive power. The main advantages are: they are available for higher voltage and power and they generate less losses since they commutate at low frequency (grid frequency).

Furthermore, inverters can also be classified depending on their number of levels:

- Low voltage applications: two levels
- Voltage increases: several semiconductors placed in series (multilevel technologies).

5. System description

In this chapter the different elements composing the studied system will be presented. Mainly, the system analysed is based on a microgrid. The main elements of the microgrid studied are: a renewable generation system, a storage generation system a constant load simulating an electrical demand and of course, the grid. A scheme of the microgrid is sketched in Figure 5.1.

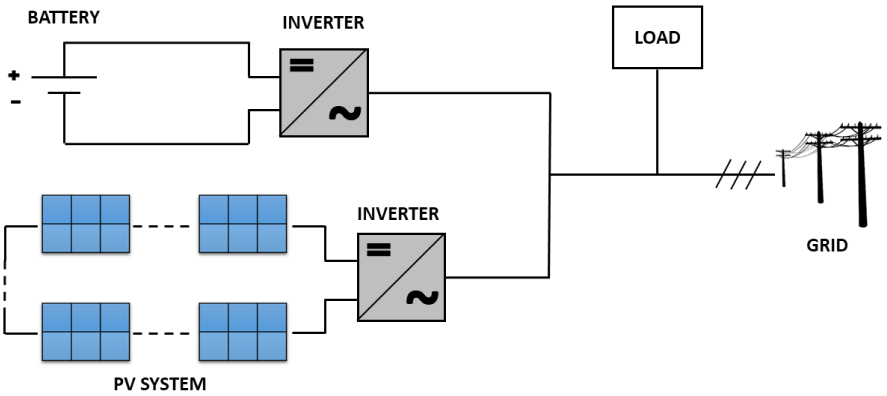

Figure 5.1 Scheme of the microgrid analysed in the present project.

The renewable generation system will consist in a photovoltaic system and the storage generation system will be a battery. Both generation systems are operated on DC current and voltage, therefore, in order to be connected to the AC grid system, it will be necessary to use inverters.

The present project, as recently mentioned, uses a grid-connected system according to the mode of operation, which means that the load could be supplied either by the PV system/battery system or the grid. According to the implementation topology, the inverter will be a central inverter. Regarding to the kind of semiconductor used the inverter will be based on insulated-gate bipolar transistors (IGBT) which provides fast switching and modulate any desired voltage. For this reason, the resulting converters applied are the Voltage Source Converters (VSC).

Two-level VSC will be used, they exchange power between the AC side and the DC side. Appropriate modulation of the IGBT switching allows to generate the desired 3-phase voltages on the AC side to control the active and reactive power flow.

Electric cables will be considered ideals, therefore, losses in the electric cables due to conduction will be neglected.

5.1. Microgrid

A microgrid is a discrete energy system consisting of distributed energy sources (demand management, storage and generation) and loads capable of operating in parallel with, or

independently from, the main power grid. The main purpose is to ensure local, reliable, and affordable energy security for urban and rural communities.

Microgrids are smaller versions of the traditional power grid. Like current electrical grids, they consist on power generation, distribution and controls (voltage regulation, switch gears). However, microgrids differ from traditional generation electrical grids by providing a closer proximity between power generation and power use, resulting in efficiency increases and transmission reductions. Another benefit is that microgrids also integrate with renewable energy sources such as solar, wind power, small hydro, geothermal, biomass and combined heat and power systems, minimizing carbon footprint and greenhouse gas emissions.

Finally, microgrids perform dynamic control over energy sources, enabling autonomous and automatic self-healing operations. During normal or peak usage, or at times of the primary power grid failure, a microgrid can operate independently and are capable of feeding power back to the main grid [13].

5.1.1. Photovoltaic system

The renewable generation system, as mentioned, will consist on photovoltaic solar panels connected in series and parallel, all of them building a PV system controlled by a central inverter. A simplified scheme of the renewable generation system is sketched in Figure 5.2.

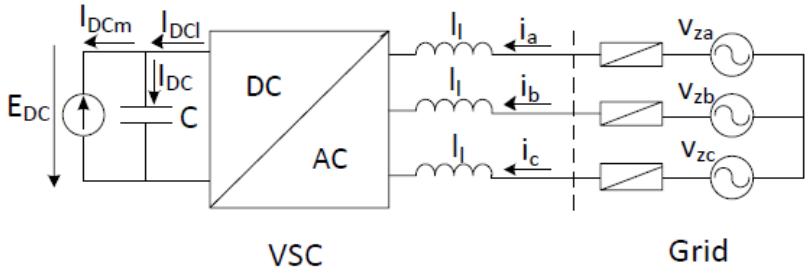

Figure 5.2 Simplified scheme of the renewable generation system: PV system modelled as a current source connected to the VSC by means of a shunt capacitor. Source: [12]

The connection between the DC side of the converter and the PV modules called DC bus current, a shunt capacitor is introduced to keep the voltage constant and therefore ensuring the power balance between the grid AC side and the DC PV system side.

As observed, the renewable generation system in this case will be modelled as a current source and the shunt capacitor.

5.1.2. Battery system

The storage system will consist on a battery. In that case, the battery system will be connected to

the DC side of the converter as a constant voltage source. See Figure 5.3.

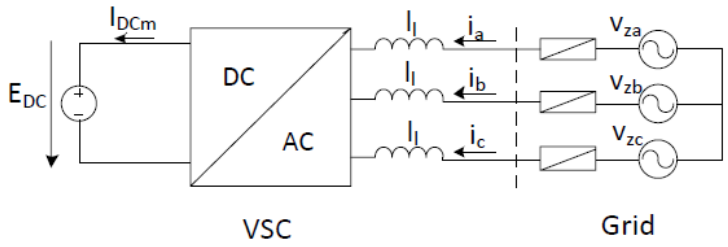

Figure 5.3 Simplified scheme of the storage system: battery system modelled as a voltage source. Source: [12]

Finally, mention that both systems: PV system and battery system, are connected to the AC grid by means of inductors that act as a filters to allow to connect smoothly the converter to the grid.

In the following chapters the modelling and control of the different elements of the microgrid will be described.

6. System Modelling

The present chapter aims to describe the modelling of the different elements of the studied system in order to simulate them later with a software tool (MATLAB Simulink 8.5). First, the entire PV system will be modelled. Later on, the modelling of the VSC will be explained. At the end, the battery system, the load and the demand models will be described shortly due to they have been modelled without being extremely laborious since they are secondary elements of the scope of the project.

6.1. Photovoltaic System Modeling

The model of a photovoltaic solar cell is mainly based on the model from Walker [14]. As presented before in section 4.2.2 Figure 4.7, the main equation to obtain the current versus the voltage of the cell is the equation (6.1).

$$I = I_L - I_0 \exp\left[\frac{q(V+IR_S)}{nkT}\right] - \frac{V+IR_S}{R_{SH}} \tag{6.1}$$

$I = current\ obtained\ from\ the\ cell(A)$

$I_L = photo\ current(A)$

$I_0 = diode\ saturation\ current(A)$

$V = voltage\ through\ the\ cell(V)$

$R_s = serie\ resistance(\Omega)$

$R_{SH} = shunt\ resistance(\Omega)$

$q = electron\ charge\ (C)$

$k = Boltzmann's\ constant\ (\frac{m^2 kg}{s^2 K})$

$n = diode\ quality/ideality\ factor$

$T = temperature\ of\ the\ cell(K)$

However, Walker [14] uses a model of moderate complexity in order to obtain a model closer to the reality. The equations used to describe accurately the IV characteristics of the cell are the following ones:

$$I_L = G\frac{I_{sc(T1)}}{G_0}\left(1 + K_0(T - T_1)\right) \tag{6.2}$$

$$K_0 = \frac{I_{sc(T2)} - I_{sc(T1)}}{T_2 - T_1} \tag{6.3}$$

$$I_0 = Id_0 \left(\frac{T}{T_1}\right)^{3/n} \exp\left(-\frac{q}{nk} V_g \left(\frac{1}{T} - \frac{1}{T_1}\right)\right) \tag{6.4}$$

$$Id_0 = \frac{I_{sc(T1)}}{\exp\left(\frac{q}{nk} \frac{V_{oc(T1)}}{T1} - 1\right)} \tag{6.5}$$

$G = irradiance\ (W/m^2)$

$V_g = band\ gap\ voltage\ (eV)$

$I_{sc(T1)}, I_{sc(T2)}, V_{oc(T1)}, T_2, T_1, G_0 = constants\ from\ the\ manufacturers' ratings$

All the constants in the above equations can be determined by examining the manufacturers' ratings of PV array and the measured IV curves of the array. Walker [14] used a PV module from the time the paper was written (2001), in order to obtain more updated results, in this project, a SunPower E19/245 W [22] array will be used to illustrate and verify the model as well as for the simulation of the microgrid later on.

From equation (6.2) it can be observed that the photocurrent (I_L) is directly proportional to irradiance (G), more sunlight means more irradiance and therefore, the photocurrent increases. When the cell is short-circuited, negligible current flows in the diode. Hence the proportionality constant in equation (6.2) is set so the rated short circuit current ($I_{SC(T1)}$) is delivered under rated irradiation (usually 1 Sun = 1000 W/m² = G_0).

Likewise, from equation (6.2), the relationship between the photo-current and temperature is linear and is deduced by noting the change of photocurrent with the change of temperature in equation (6.3).

From equation (6.1), when the cell is not illuminated (I_L=0), the relationship between the cell's terminal voltage and current is given by the diode equation. When the cell is open-circuited (I=0) and illuminated ($I_L \neq 0$), the photocurrent flows entirely in the diode.

The relationship of the saturation current (I_0) with the temperature is complex (equation (6.4)) and it is out of the scope of the project, fortunately it contains no variables requiring evaluation.

Last, the value of the saturation current at 25°C is calculated using open-circuit voltage and short-circuit voltage at this temperature (equation (6.5)).

In case of connecting cells in series or in parallel, from theory, series connection maintains the short circuit current constant meanwhile voltage adds up proportionally (equation (6.7)). Likewise, parallel connection maintains the open circuit voltage constant meanwhile intensity

adds up proportionally (equation (6.8)).

$$V_{OC,Ns} = Ns \cdot V_{OC} \tag{6.7}$$

$$I_{SC,Np} = Np \cdot I_{SC} \tag{6.8}$$

The following MATLAB script introduces all the parameters (Figure 6.1) and makes some initial calculations. The Simulink model of the solar cell is sketched in Figure 6.2.

```
%Matlab script for the PV model SunPower E19/245
Temp=298; %Temperature K (free parameter)
G0=1000; %Irradiance w/m2 (free parameter)
Rs=0.4804/72; %Rseries ohm
Rsh=370.7525; %Rshunt ohm
n=0.92671; %diode quality factor
Kboltz=1.38e-23; %Boltzmann's constant m2 kg s-2 K-1
Qcharge=1.6e-19; %Electron charge coulombs
QAK=Qcharge/(n*Kboltz); %Constant including Qcharge,n and Kboltz
Ns=72*1; %number of arrays connected in series (72 cells/array)
Np=1; %number of arrays connected in parallel

%SunPower E19/245 module data
T1= 273+25; % T(K)
Voc_T1=48.8/72; % (V)one cell
Isc_T1=6.43; % (A)
T2=273+45; % T(K)
Voc_T2=46.32/72; % (V)one cell
Isc_T2=6.48;%(A)

Id0=Isc_T1/(exp(QAK*Voc_T1/T1)-1);
K0=(Isc_T2-Isc_T1)/(T2-T1);
Vg=1.12; % bandgap voltage from Walker
ILConst= Isc_T1/G0; %proportionality constant I/G- [A/(wm-2)]
```

Figure 6.1 Matlab script of the PV model SunPower E19/245

In order to validate the model and verify its functionality some simulations were carried out showing the effect to the IV curve (and consequently to the PV curve) by the irradiance (Figure 6.3), the temperature (Figure 6.4) and the number of arrays connected in series (Figure 6.5) or in parallel (Figure 6.6).

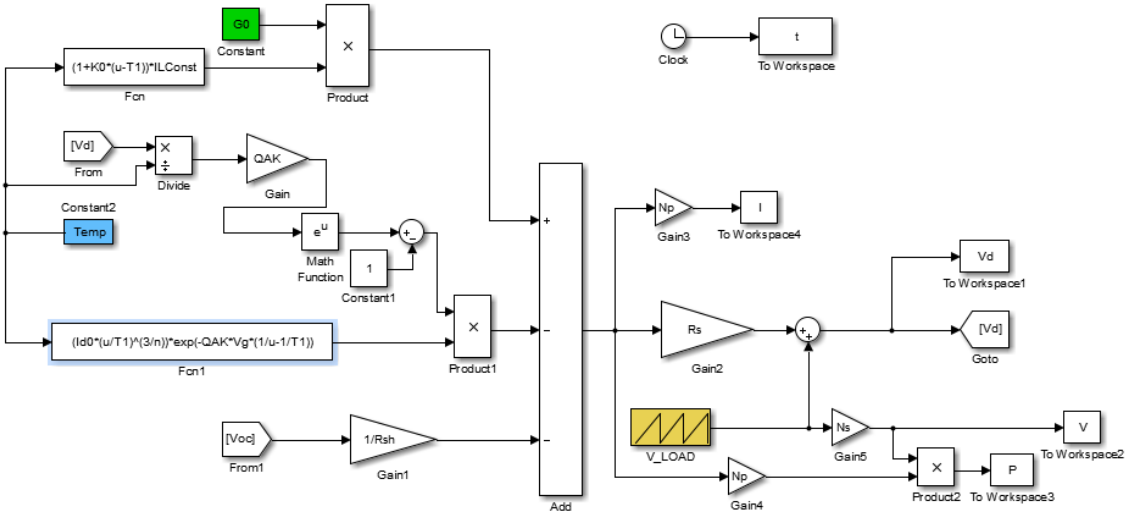

Figure 6.2 Simulink model of the photovoltaic system based on [15].

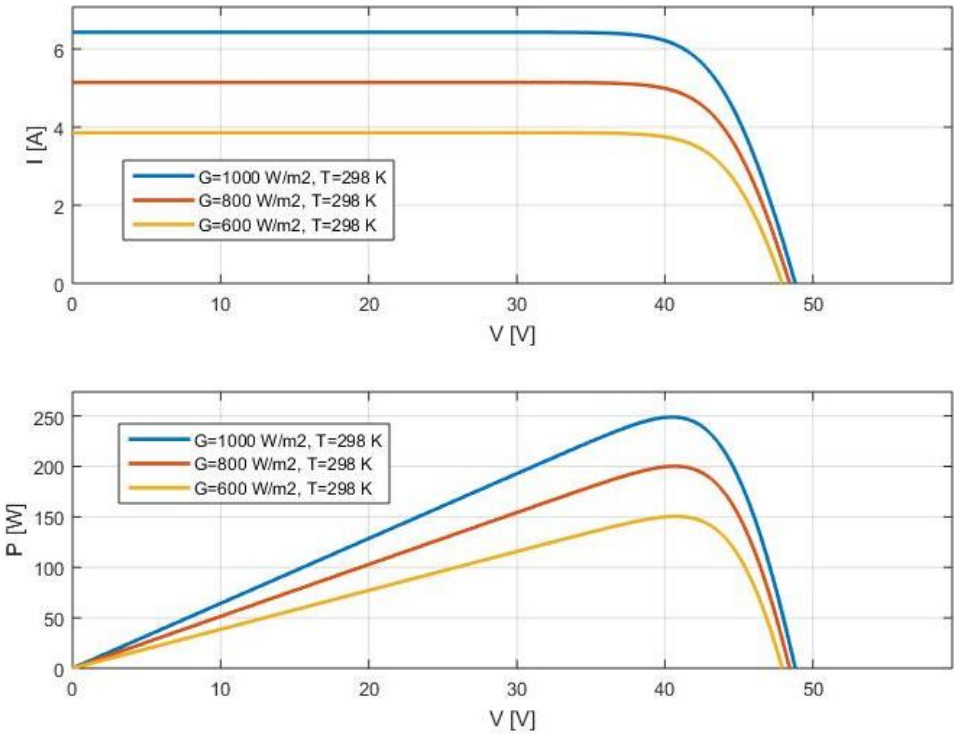

Figure 6.3 Effect of the light intensity (G) on the IV curves and PV curves. Higher irradiance means higher power.

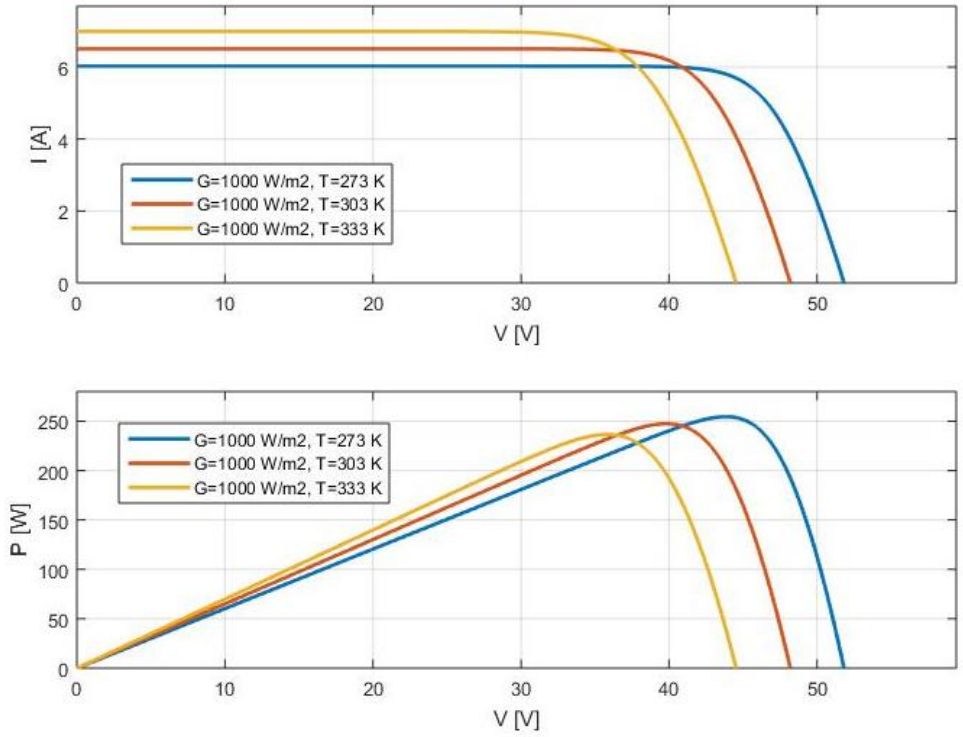

Figure 6.4 Effect of the temperature (T) on the IV and PV curves. Warmer temperatures means lower power.

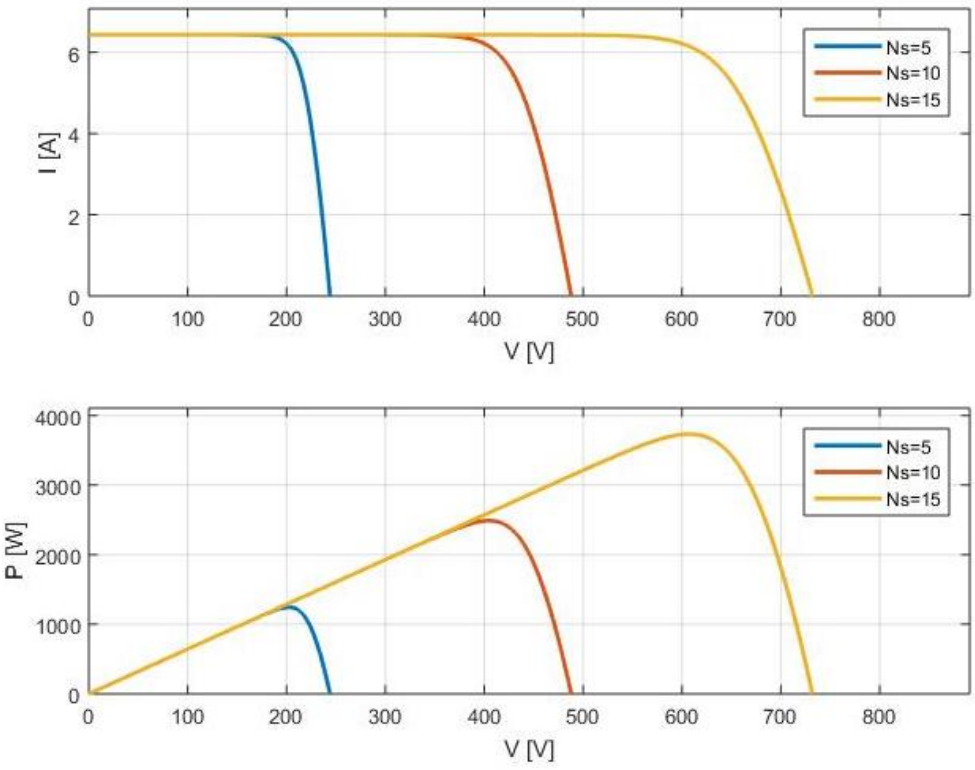

Figure 6.5 IV and PV curves with different number of PV arrays placed in series. It verifies equation 6.7.

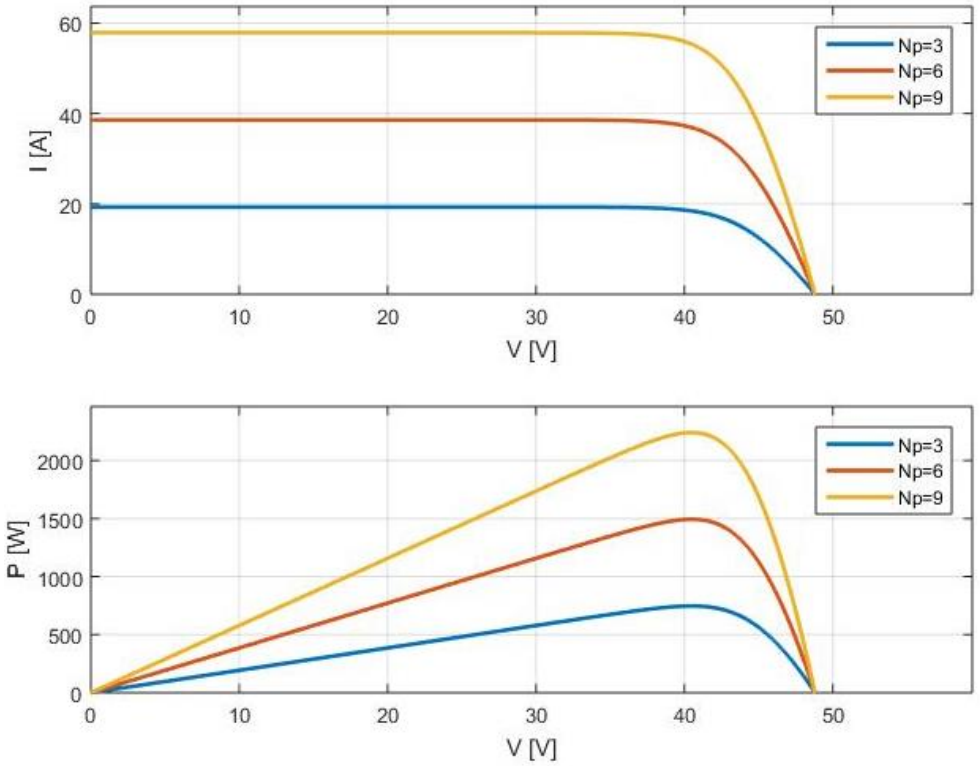

Figure 6.6 IV and PV curves with different number of PV arrays placed in parallel. It verifies equation 6.8.

6.2. Voltage Source Converter Modelling

The VSC used for this project are AC/DC inverter. They connect a DC system to an AC system. As mentioned before, a two-level VSC will be applied. They are built using six IGBTs (two IGBTs each phase). However, to simplify the control of the VSC, an ideal simplified model of the VSC will be used. This simplified model divides the VSC in two sides: DC side and AC side [12]. AC side is modelled as three-phase controlled voltage sources and the DC side is modelled as a controlled current source (Figure 6.7).

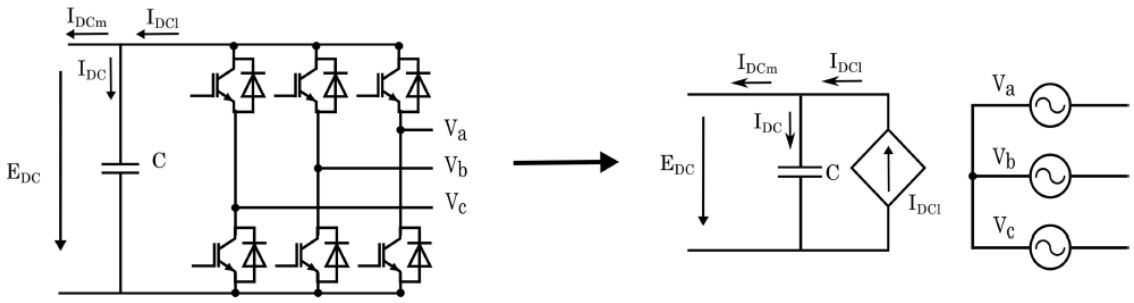

Figure 6.7 Left: real model of a VSC. Right: simplified model of a VSC. Source: [12]

Both sides of the converter (DC and AC) are linked in order to guarantee the power balance. All the power generated from the DC side are injected to the AC side and vice versa. Thus, the value

of the controlled current source on the DC side can be expressed as equation (6.9).

$$I_{DCl} = \frac{P_{AC}}{E_{DC}} \tag{6.9}$$

Where:

$I_{DCl} = intensity\ of\ the\ current\ source\ from\ the\ DC\ side\ of\ the\ converter$

$P_{AC} = power\ from\ the\ AC\ side\ of\ the\ converter$

$E_{DC} = voltage\ from\ the\ DC\ side$

In order to connect the AC side of the converter to the main grid it is necessary to use inductors with their resistance associated between the voltage sources to avoid to connect sources of the same kind, which could produce short circuits (Figure 6.8). This way, the voltage sources are converted to current sources.

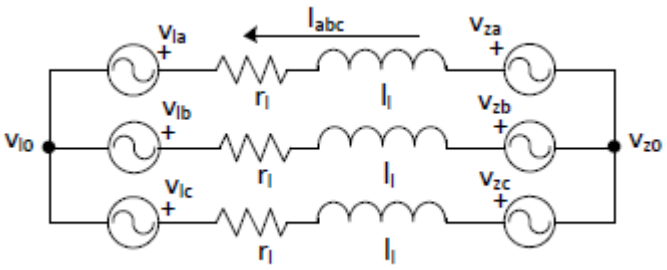

Figure 6.8 Equivalent model of the AC side of the VSC converter. Source: [12].

Applying Kirchhoff's laws, the voltage equation of the AC side of the VSC converter can be obtained (equation (6.10)). Likewise, applying Park's transformation (Appendix A) and taking into account that for three-wire systems $i_0 \equiv 0$, the voltage equation in qd0 reference system are obtained (equation (6.11)).

$$\begin{bmatrix} v_{za} \\ v_{zb} \\ v_{zc} \end{bmatrix} - \begin{bmatrix} v_{la} \\ v_{lb} \\ v_{lc} \end{bmatrix} - (v_{l0} - v_{z0}) \begin{bmatrix} 1 \\ 1 \\ 1 \end{bmatrix} = \begin{bmatrix} r_l & 0 & 0 \\ 0 & r_l & 0 \\ 0 & 0 & r_l \end{bmatrix} \begin{bmatrix} i_a \\ i_b \\ i_c \end{bmatrix} + \begin{bmatrix} l_l & 0 & 0 \\ 0 & l_l & 0 \\ 0 & 0 & l_l \end{bmatrix} \frac{d}{dt} \begin{bmatrix} i_a \\ i_b \\ i_c \end{bmatrix} \tag{6.10}$$

Where:

$v_{za}, v_{zb}, v_{zc} = three\ phase\ instantaneous\ grid\ voltages\ in\ the\ abc\ frame$

$v_{la}, v_{lb}, v_{lc} = three\ phase\ instantaneous\ converter\ voltages\ in\ the\ abc\ frame$

$i_a, i_b, i_c = three\ phase\ instantaneous\ currents\ in\ the\ abc\ frame$

$r_l = inductance\ equivalent\ resistance$

$l_l = inductance\ value$

$v_{l0} - v_{z0} = voltage\ difference\ between\ the\ converter\ and\ the\ grid\ neutrals.$

$In\ the\ case\ of\ a\ balanced\ system\ without\ neutral\ conductor\ its\ value\ is\ zero.$

$$\begin{bmatrix} v_{zq} \\ v_{zd} \end{bmatrix} - \begin{bmatrix} v_{lq} \\ v_{ld} \end{bmatrix} = \begin{bmatrix} r_l & -l_l\omega_e \\ l_l\omega_e & r_l \end{bmatrix} \begin{bmatrix} i_q \\ i_d \end{bmatrix} + \begin{bmatrix} l_l & 0 \\ 0 & l_l \end{bmatrix} \frac{d}{dt} \begin{bmatrix} i_q \\ i_d \end{bmatrix} \quad (6.11)$$

$v_{zq}, v_{zd} = grid\ qd0\ frame\ voltages$

$v_{lq}, v_{ld} = converter\ qd0\ frame\ voltages$

$i_q, i_d = qd0\ frame\ currents$

$\omega_e = electrical\ angular\ velocity$

Following the same logic, in order to connect the DC side of the converter to a PV system modelled as a current source, a capacitor connected in parallel is necessary to convert the controlled current source into a voltage source (as can be seen in Figure 6.7). However, if the DC side of the converter is connected to a battery (voltage source), then, it would not be necessary to use a capacitor.

6.3. Battery system and Load Modelling

Batteries are electrochemical devices that convert chemical energy into electrical energy. For the present work a battery system of constant DC voltage is assumed. Therefore, the battery has been modelled as a simple controlled voltage source (see Figure 5.3 from section 5.1.2).

The constant load will be modelled as three resistances connected to the main grid (Figure 6.9). Therefore, the load only consumes active power.

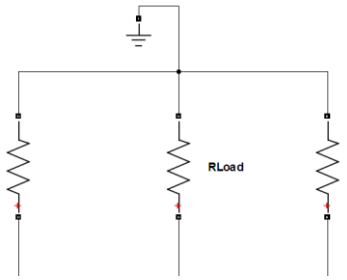

Figure 6.9 Three resistances RLoad one for each phase simulating a constant load.

Finally, ideal transmission lines have been considered, thus, no resistance neither inductors has been added to simulate the real conduction losses in the transmission lines, since they do not usually represent a big percentage and do not affect heavily the behaviour of the microgrid.

The following chapter will present the control methods for the microgrid proposed.

7. System Control

This chapter will explain the control methodologies applied to the different elements modelled in the previous chapter. The control of the PV system and its converter will be the first one. The control of the Battery system and its converter will be the second one.

7.1. Photovoltaic System Control

7.1.1. VSC control PV side

The control of the VSC on the PV side allows to control the power generated from the PV modules, this is the power that will be transferred to the VSC on the DC side and lately injected to the grid.

As mentioned earlier, the performance of a PV cell depends on two variables climate factors: irradiance and temperature. The other factors referring the quality of the cell or the sizing of the PV system are fixed variables once installed. As seen in section 6.1, the IV curves of a solar cell changes with the light intensity (G) and temperature (T). However, only the change of temperature changes the open circuit voltage value. Therefore, it is essential to make the PV system work to the point of maximum power for every temperature, which is the knee of the IV curve.

The solution is to implement a MPPT algorithm, it will track the voltage from the IV curve that gives the maximum power and having the voltage at maximum power the PV module will determine automatically the current at maximum power.

Summarizing, the control of the VSC on the PV side is sketched in Figure 7.1, where the inputs to the PV module are the irradiance (G), temperature (T) and voltage from the DC side (E_{DC}, given by equation (6.9) seen in section 6.2) and the output is the current flowing through the cell ($-I_{DCm}$). The input for the MPPT block is the temperature (T) and its output will be the voltage at maximum power V_{mpp} that is the desired voltage for the DC side (E_{DC}*).

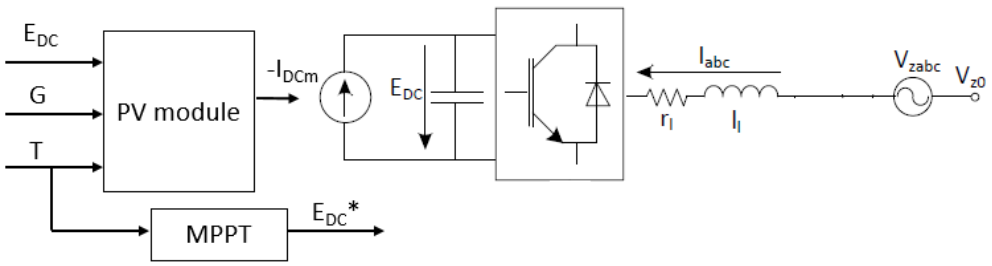

Figure 7.1 PV VSC converter control scheme.

7.1.1.1. MPPT Algorithm

There are several methods to implement MPPT [16]. The three most common MPPT algorithms are [17]:

- Perturbation and observation (P&O): this algorithm perturbs the operating voltage to ensure maximum power.
- Incremental conductance: this algorithm compares the incremental conductance to the instantaneous conductance in a PV system. Depending on the result, it increases or decreases the voltage until the MPP is reached. Unlike with the P&O algorithm, the voltage remains constant once MPP is reached.
- Fractional open-circuit voltage: this algorithm is based on the principle that the maximum power point voltage is always a constant fraction of the open circuit voltage. The open circuit voltage of the cells in the PV array is measured and used as input to the controller.

The present project applies the last algorithm due to it is effective and less laborious to implement. The Simulink MPPT algorithm is sketched in Figure 7.2.

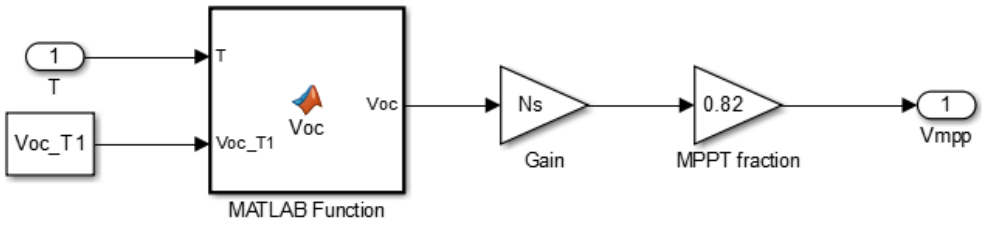

Figure 7.2 Simulink MPPT algorithm block. It is based on the method Fractional Open Circuit Voltage.

The Matlab Function block with temperature (T) and open circuit voltage at 25°C of one cell as inputs, applies equation (7.1) [18] to obtain the open circuit voltage at the given temperature (T) as output. For the SunPower E19/245 PV module the temperature coefficient is $\beta = -0{,}254\ \%/°C$. Then, it is multiplied by the total number of modules connected in series due the previous result is calculated only for one cell, and finally, it is multiplied by the MPPT fraction (normally a value between 0,7-0,82 [16]) and the maximum power point voltage for temperature (T) is obtained.

$$V_{OC(T)} = V_{OC_{T_1}}\left(1 + \beta(T - 25°C)\right) \tag{7.1}$$

$V_{OC(T)} = open\ circuit\ voltage\ at\ temperature\ T\ in\ V$

$V_{OC_{T_1}} = open\ circuit\ voltage\ at\ temperature\ T1(25°C)\ in\ V$

$\beta = temperature\ coefficient\ in\ \%/°C\ \ of\ V_{OC}$

$T = temperature\ in\ °C$

7.1.2. VSC control grid side

As mentioned previously, VSC converters are able to control separately active and reactive power. Normally, the reactive power reference can be obtained from a higher level control system, for example, grid operator, or set to a given value. The active power reference for the case of a renewable energy system as the PV system, it is adjusted to regulate the DC bus voltage in order to ensure power balance. Hence the power injected into the grid will be the same as the generated power [12].

The control scheme for this converter is sketched in Figure 7.3. It is based on two level cascaded control system. The inner level controller allows to regulate the AC current in the $qd0$ reference (current loop), while the outer level controller allows to regulate the DC bus voltage in the $qd0$ reference as well (voltage loop).

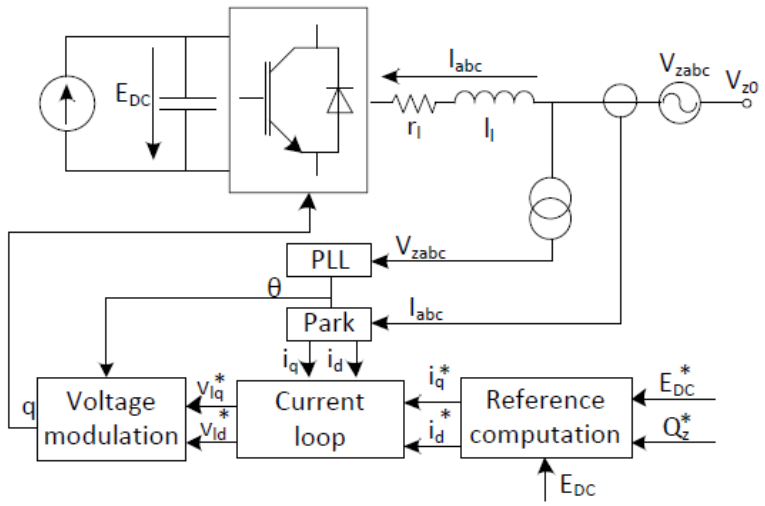

Figure 7.3 Control scheme of VSC grid side for renewable energy system. Source: [12]

The different controllers deal with current and voltages in the $qd0$ rotating two-axis reference frame to adjust the electrical grid angle. Due to this fact, a Phase Locked Loop (PLL) to track the grid angle is required. This grid angle will be used to carry out all the Park and Anti-Park transformations needed to control the system.

The following sections will follow the control scheme starting with the design of the PLL, then, the reference computation, the current loop and in the end the voltage modulation.

7.1.2.1. Design of the Phase Locked Loop (PLL)

A phase locked loop (PLL) is used to determine the angle and the angular velocity of the electrical network. The design of a typical PLL controller is elaborated using the methodology explained by Chung [19]. A PLL control scheme is shown in Figure 7.4. It consists in a feedback of the d-axis

voltage component filtered by a PI controller. The output of the controller is the estimated angular velocity of the electrical grid $\hat{\omega}$ and its integration gives the estimated grid angle $\hat{\theta}$.

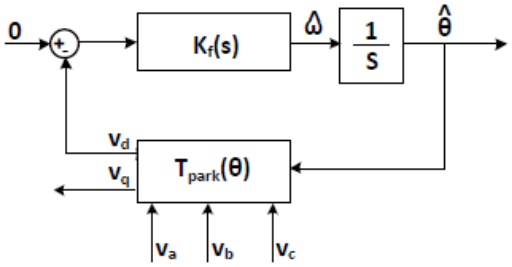

Figure 7.4 Phase Locked Loop controller scheme. Source: [12]

Assuming the angle error to be small, the system can be linearized and modelled as a second order system [12] (equation (7.2)).

$$\frac{\hat{\theta}(s)}{\theta(s)} = \frac{2\xi\omega_e s+{\omega_e}^2}{s^2+2\xi\omega_e+{\omega_e}^2} \tag{7.2}$$

Where $\hat{\theta}(s)$ is the estimated grid angle and $\theta(s)$ is the real grid angle. The PLL PI controller can be defined as equation (7.3).

$$K_f = K_p\left(\frac{\frac{1}{\tau_{PLL}}+s}{s}\right) = K_p + \frac{Kp}{\tau_{PLL}}\frac{1}{s} \tag{7.3}$$

Where τ_{PLL} is the PLL time constant.

The controller parameters K_p and τ_{PLL} can be computed using the following expressions (7.4) and (7.5).

$$\omega_e = \sqrt{\frac{K_p E_m}{\tau_{PLL}}} \tag{7.4}$$

$$\xi = \frac{\sqrt{\tau_{PLL}K_p E_m}}{2} \tag{7.5}$$

Where E_m is the admitted peak voltage value, ξ is the damping ratio, ω_e is the electrical angular velocity.

The following example to test the PLL has been carried out using $\omega_e = 2\pi 50\ rad/s$, $E_m = 400\sqrt{2}/\sqrt{3}\ V$ and $\xi = 0.707$. Applying the last two expressions the values of $\tau_{PLL} = 0{,}0045\ s$ and $K_p = 1{,}3601$ are computed. The results are shown in Figure 7.5.

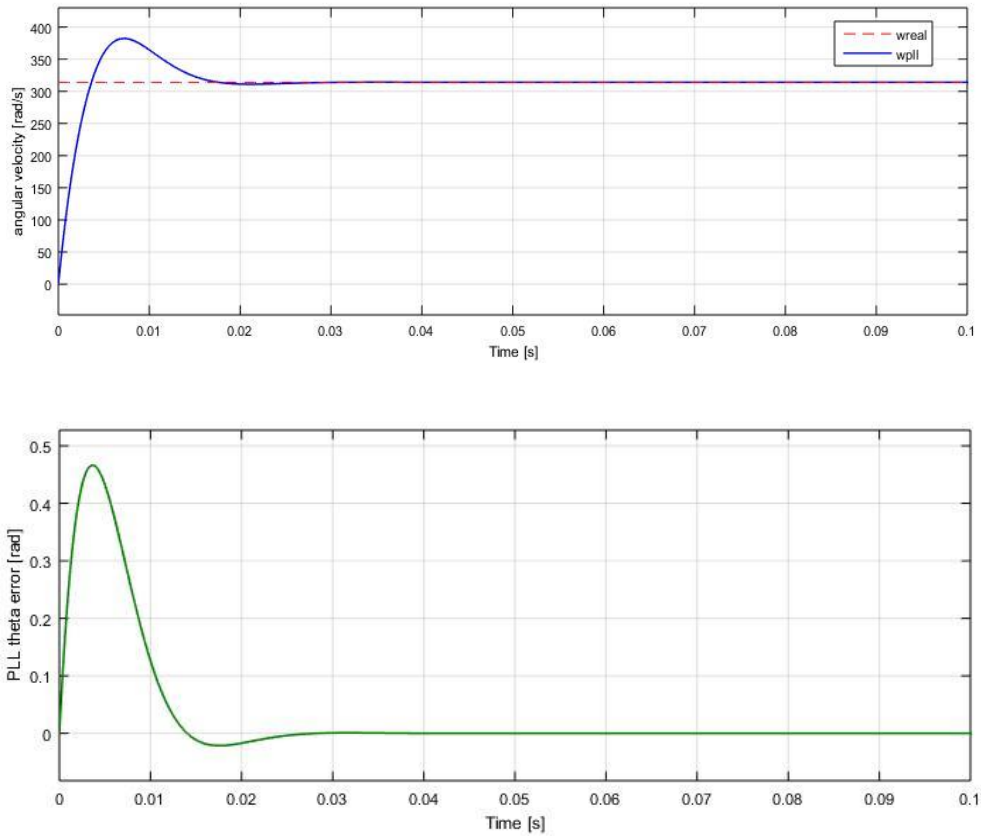

Figure 7.5 Upper graph: electrical angular velocity real (red) vs estimated (blue). Lower graph: PLL angle error = real grid angle minus estimated grid angle.

7.1.2.2. Reference computation

In order to obtain the current references i_q^* and i_d^* from the desired active and reactive powers P* and Q*, the Instantaneous Power Theory mentioned in the Appendix A will be used [12].

$$P^* = \frac{3}{2}\left(v_{zq} i_q^* + v_{zd} i_d^*\right) \tag{7.6}$$

$$Q^* = \frac{3}{2}\left(v_{zq} i_d^* + v_{zd} i_q^*\right) \tag{7.7}$$

Rearranging equations (7.6) and (7.7) and taking into account that the PLL described earlier ensures that $v_{zd} = 0$, equations (7.8) and (7.9) are obtained.

$$i_q^* = \frac{2}{3}\frac{P^*}{v_{zq}} \tag{7.8}$$

$$i_d^* = \frac{2}{3}\frac{Q^*}{v_{zq}} \tag{7.9}$$

As mentioned before, the desired reactive power Q* will be set to a given value and the active power P* will be adjusted to regulate the DC bus voltage. Therefore, in order to obtain the value

of active power, a voltage loop is needed to control the DC bus voltage; v_{zq} will be obtained from the grid applying a Park transformation.

7.1.2.2.1 Design of the Voltage Loop

The voltage loop or DC voltage regulator is required to control the voltage of the DC bus ensuring power balance between the PV generation source and the power injected into the grid. The output of the DC voltage controller will provide the active power P* and applying equation (7.8) the i_q^* reference for the current loop will be obtained.

The control scheme of the voltage loop is sketched in Figure 7.6. The controlled quantity is E_{DC}^2 due to it is proportional to the energy stored in the capacitor, it is first compared to the desired bus voltage power two $E_{DC}^{2^*}$. The desired bus voltage is set to the MPP to extract the maximum power that the PV system can generate. A feed-forward scheme is used to improve the system response [12]. The output of the controller is the active power injected to the capacitor P_C^*.

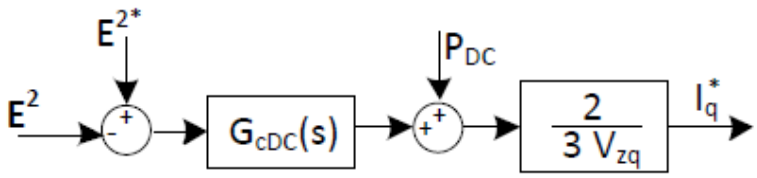

Figure 7.6 Voltage loop controller scheme of the VSC grid side. Source: [12]

This power then it is added with the active power measured before the capacitor P_{DC} and the result power is the power reference for the converter (equation 7.10), the power that the VSC has to inject from the grid to the bus to obtain the desired bus voltage.

$$P^* = P_C^* + P_{DC} \tag{7.10}$$

$P^* = power\ reference\ for\ the\ power\ converter$

$P_C^* = active\ power\ that\ should\ be\ injected\ to\ the\ capacitor$

$P_{DC} = measured\ power\ before\ the\ capacitor = -I_{DCm} \cdot E_{DC}$

The controller applied to the voltage loop can be a proportional (P) controller or a proportional-integral controller (PI). The present projects uses a PI controller.

In order to design the PI controller, equation (7.11) is used. It shows the capacitor power in the Laplace domain.

$$P_C(s) = \frac{1}{2} sC E_{DC}^2(s) \tag{7.11}$$

$P_C = capacitor\ power$

$C = capacitor\ capacitance$

Then, the transfer function between the capacitor power and the DC bus voltage can be described as equation (7.12).

$$S(s) = \frac{E_{DC}^2(s)}{P_C(s)} = \frac{2}{sC} \tag{7.12}$$

To have no steady state error a controller must have integral action. It is therefore natural to use a PI controller which has the following transfer function (equation (7.13)).

$$G_{C_{DC}}(s) = K_{PDC} + \frac{K_{iDC}}{s} \tag{7.13}$$

The transfer function of the closed system applying the PI controller is computed as equation (7.14).

$$W(s) = \frac{S(s)G_{C_{DC}}(s)}{1+S(s)G_{C_{DC}}(s)} = \cdots = \frac{sK_{PDC}+K_{iDC}}{\frac{1}{2}s^2C+sK_{PDC}+K_{iDC}} \tag{7.14}$$

Comparing equation (7.14) which is of the form of the normalized transfer function of a second order system as shown in equation (7.15), the PI controller gains can be computed as equation (7.16) and (7.17).

$$W(s) = \frac{2s\xi_E\omega_E+\omega_E^2}{s^2+2s\xi_E\omega_E+\omega_E^2} \tag{7.15}$$

$$K_{PDC} = C\xi_E\omega_E \tag{7.16}$$

$$K_{iDC} = \frac{C\omega_E^2}{2} \tag{7.17}$$

Where ξ_E is the desired damping ratio of DC voltage loop, ω_E is the desired angular velocity of the voltage loop and C is the value of the capacitor of the converter DC side.

Last detail of the voltage loop is that as mentioned before, it is the outer level of the two-level cascaded control system, therefore, it has to be considerably slower than the inner level, which is the current loop, in order to ensure system stability.

7.1.2.3. Design of the Current Loop

The current loop has the purpose to determine the voltages that the VSC has to apply in order to ensure that the currents flowing through the converter are the same as the required by the control. That is from the real currents flowing through the converter i_q and i_d and from the required currents i_q^* and i_d^* computed on the reference computation block, the current loop

calculates the voltages v_{lq} and v_{ld} needed to ensure both currents are equal.

A scheme of the current loop controller is sketched in Figure 7.7.

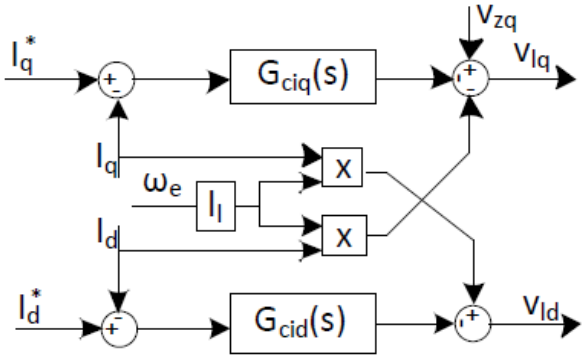

Figure 7.7 Scheme of the current loop controller. Source: [12]

By assuming $v_{zd} = 0$ due to the properly performance of the PLL described earlier, the voltage equations from the equations (6.11) (Section 6.2) can be written as (7.18).

$$\begin{bmatrix} v_{zq} \\ 0 \end{bmatrix} - \begin{bmatrix} v_{lq} \\ v_{ld} \end{bmatrix} = \begin{bmatrix} r_l & -l_l\omega_e \\ l_l\omega_e & r_l \end{bmatrix} \begin{bmatrix} i_q \\ i_d \end{bmatrix} + \begin{bmatrix} l_l & 0 \\ 0 & l_l \end{bmatrix} \frac{d}{dt} \begin{bmatrix} i_q \\ i_d \end{bmatrix} \tag{7.18}$$

From the equations (7.18) it can be observed that the voltage components depend both of them (v_q and v_d) of i_q and i_d. To control q and d components separately it is necessary to decouple them as in (7.19).

$$\begin{bmatrix} v_{lq} \\ v_{ld} \end{bmatrix} = \begin{bmatrix} v_{zq} - l_l\omega_e i_d - \hat{v}_{lq} \\ l_l\omega_e i_q - \hat{v}_{ld} \end{bmatrix} \tag{7.19}$$

Where $\hat{v}_{lq}$ and $\hat{v}_{ld}$ are the outputs of the controllers and they are defined from (7.18) and (7.19) as (7.20).

$$\begin{bmatrix} \hat{v}_{lq} \\ \hat{v}_{ld} \end{bmatrix} = \begin{bmatrix} r_l & 0 \\ 0 & r_l \end{bmatrix} \begin{bmatrix} i_q \\ i_d \end{bmatrix} + \begin{bmatrix} l_l & 0 \\ 0 & l_l \end{bmatrix} \frac{d}{dt} \begin{bmatrix} i_q \\ i_d \end{bmatrix} \tag{7.20}$$

Applying the Laplace transformation, the transfer functions between the controller voltages and converter currents can be computed as (7.21) and (7.22).

$$\frac{i_q(s)}{\hat{v}_{lq}(s)} = \frac{1}{l_l s + r_l} = G_m(s) \tag{7.21}$$

$$\frac{i_d(s)}{\hat{v}_{ld}(s)} = \frac{1}{l_l s + r_l} = G_m(s) \tag{7.22}$$

Using the last two transfer functions and Internal Model Control technique [20] the following PI

controllers can be designed (7.23).

$$G_{C_{iq}}(s) = G_{C_{id}}(s) = K_{Pcl} + \frac{K_{icl}}{s} \tag{7.23}$$

Where the constants can be calculated as follow (7.24), (7.25) and (7.26) using a first order filter (7.27). $G_m^+(s)$ is the inverse of $G_m(s)$.

$$G_{C_{iq}}(s) = G_{C_{id}}(s) = \frac{G_f(s)G_m(s)G_m^+(s)}{1-G_f(s)G_m(s)G_m^+(s)} = \cdots = \frac{l_l}{\tau_{cl}} + \frac{r_l}{\tau s} \tag{7.24}$$

$$K_{Pcl} = \frac{l_l}{\tau_{cl}} \tag{7.25}$$

$$K_{icl} = \frac{r_l}{\tau_{cl}} \tag{7.26}$$

$$G_f(s) = \frac{1}{\tau_{cl}s+1} \tag{7.27}$$

Where τ_{cl} is the closed loop time constant of the current loop. This constant must be chosen considering the converter physical restrictions. It is usual to define it 10 times slower than the converter IGBT switching frequency.

7.1.2.4. Design of the Voltage Modulation

Until now, the control system has been the same if the working mode of the VSC converter is the simplified one or the real one (with IGBT). However, the voltage modulation is only needed for the real model.

For the simplified or ideal model, the voltages computed from the current loop in the $qd0$ reference frame are transformed to the abc reference frame with an Anti-Park transformation block and they are directly introduced to the controlled voltage sources modelled on the converter AC side (v_{la}, v_{lb}, v_{lc}).

For the real model, the voltages obtained from the current loop are also transformed into the abc reference frame. The VSC converter can apply the referenced voltages by modulating them using Pulse Width Modulation (PWM). The modulation tells the IGBT when to switch. One of the simplest technique to implement PWM is Sinusoidal Pulse Width Modulation (SPWM).

SPWM compares two signals: the desired signal or modulating signal, and a triangular signal called carrier signal. The comparison between both signals results on a square waveform signal which contains a copy of the desired signal (Figure 7.8). Note that the carrier signal frequency will be the switching frequency of the IGBT.

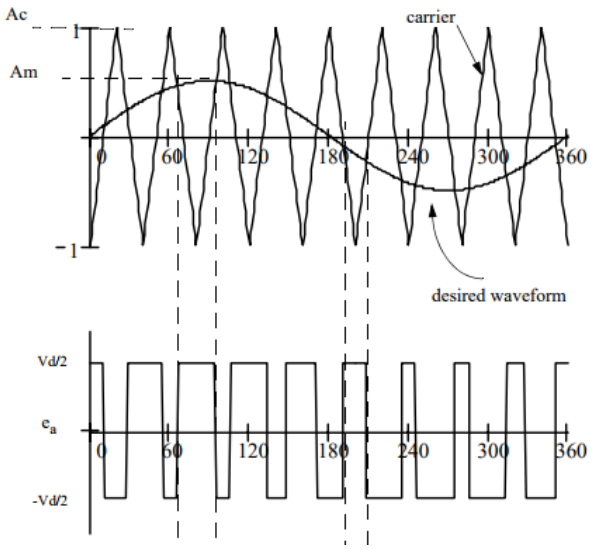

Figure 7.8 Working principle of SPWM. Source: [21]

This technique allows an easy filtering of the signal with good results. A higher carrier frequency means a more precise modulation but also means a large number of switchings per cycle and hence in an increased power loss.

When designing the SPWM there are two parameter to take into account, modulation index or relation between the amplitudes of the modulation signal and the carrier (7.28) and the relation between the frequencies of the modulation signal and the carrier (7.29) [21].

$$m = \frac{A_m}{A_c} \leq 1 \tag{7.28}$$

$$n = \frac{f_m}{f_c} = 3k, (k \in N) \tag{7.29}$$

Controlling the modulation index it also controls the amplitude of the applied output voltage. A modulation index greater than one means overmodulation, depending on the interest sometimes is allowed. For three-phase system it is advisable to use a frequency relation multiple of three allowing to use one carrier signal for the three phases. Typically, switching frequencies in the 2-15 kHz range are considered adequate for power systems applications [21].

A simulation carried out with IGBT and SPWM will be presented in the next chapter.

7.2. Battery System Control

7.2.1. VSC control Battery side

As the battery will be modelled as a controlled voltage source at a given value, no further control

is needed. Likewise, the DC side of the converter will be modelled as a controlled voltage source with a value equal to equation (6.9) in order to guarantee power balance.

7.2.2. VSC control grid side

The control scheme for the battery converter (Figure 7.9) is similar to the photovoltaic system converter seen in section 7.1.2.

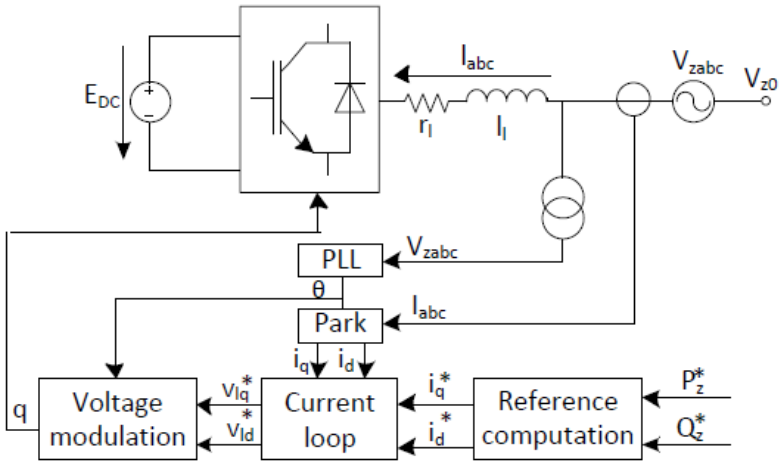

Figure 7.9 Control scheme of VSC grid side for storage system. Source: [12]

7.2.2.1. Design of the PLL

As both systems are connected to the same main grid, only a PLL design is needed, the grid angle computed will be used for all the microgrid. Therefore the design explained in section 7.1.2.1 will be implemented just once.

7.2.2.2. Reference Computation

The main difference between the converter controls of the two systems is located on the reference computation block. For the battery system, a DC voltage bus controller is not needed due to the fact that the active power reference in the storage system is adjusted to charge the battery or to inject power to the grid depending on the operation of the energy management system of the microgrid [12]; however, the mentioned energy management system is not detailed and fully studied in the present project. Therefore, the inputs of the reference computation block will be the active power and the reactive power desired and equations (7.8) and (7.9) will be directly applied to compute the currents references.

7.2.2.3. Design of the Current Loop

The design of the current loop control for the battery system will be designed exactly as for the PV

system converter described in section 7.1.2.3.

7.2.2.4. Design of Voltage Modulation

Similarly, in case of using IGBTs, the design of voltage modulation control will follow the same steps as for the PV system converter described in section 7.1.2.4.

Next chapter will deal with the simulations that have been carried out in order to test the behaviour and functionality of the different elements and the entire microgrid.

8. Simulations and results

In this chapter, the simulations carried out to test the correct behaviours of the photovoltaic system, the battery system, the converters and the entire microgrid will be exposed. First, the value of the parameters for the simulations will be presented. Secondly the results of the simulation will be shown and a brief discussion will be elaborated.

Mention that all the simulations have been carried out using MATLAB Simulink 8.5 and a schematic simplified Simulink model of the microgrid is shown in Figure 8.1. Note that the control blocks are not shown.

All the simulations have a simulation time of 1 second. Otherwise, a higher simulation time would take too long to finish it. Hence, some adjustments will need to be applied for some parameters since the present project will consider that the time units of second will follow the next rule: at 0,0 second it will be 9 am, at 0,1 second it will be 10 am, and so on. Therefore at 1,0 second it will equal to 7 pm. In other words, 0,1 second is equal to 1 hour. This selection will have an important role when modelling the temperature and light intensity parameters for the PV system; since, it is purely to make the simulation a bit more familiar to the reality.

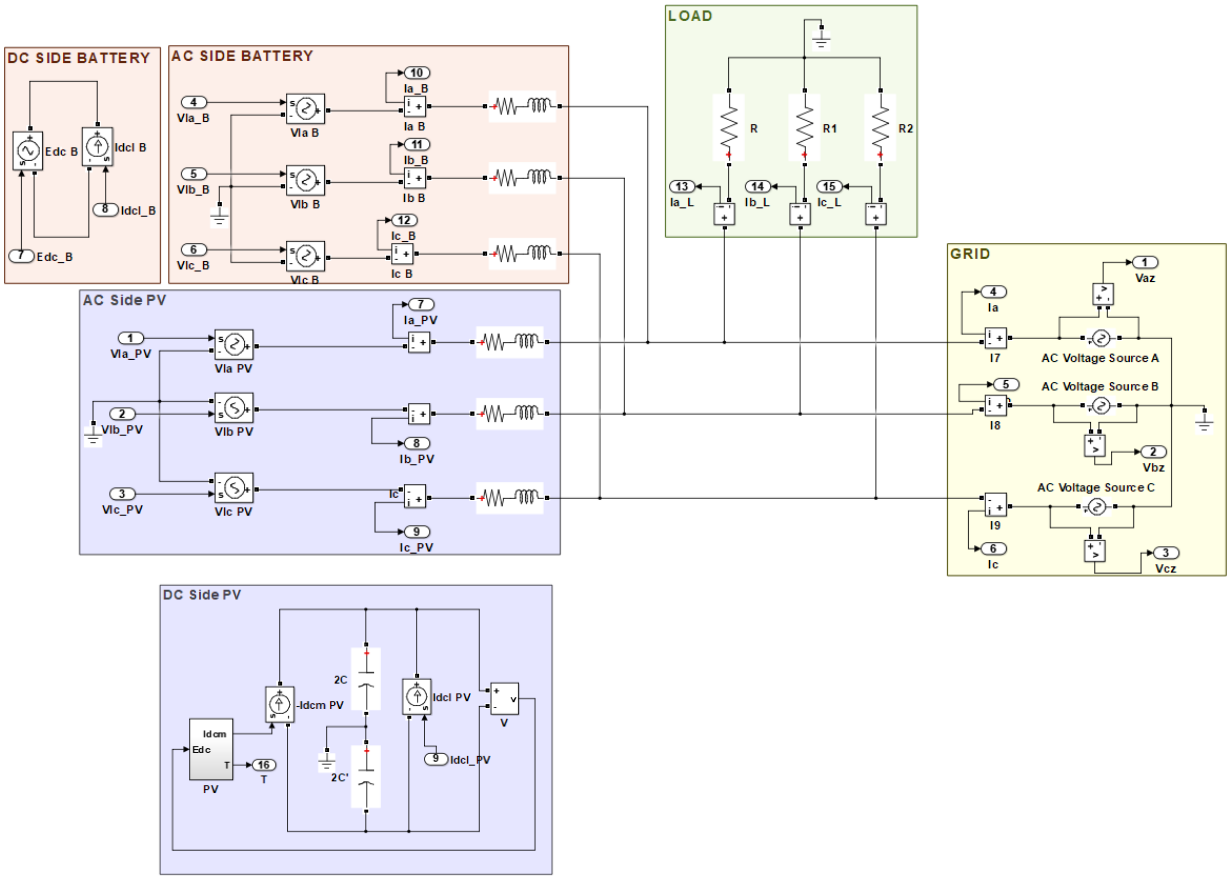

Figure 8.1 Simulink general model of the microgrid without the control blocks.

8.1. Parameters

Both physical elements parameters and control parameters (if needed) for the different systems will be presented below. Whether for any simulation a parameter needs to be changed it will be mentioned when describing the simulation.

8.1.1. Grid parameters

The grid considered is a European AC three phase grid of 400 V and 50 Hz (Figure 8.2). Therefore the peak amplitude is $E_m = 400\sqrt{2}/\sqrt{3}\,V$and the electrical grid angular velocity is $\omega_e = 2\pi 50\,rad/s$. These parameters values will also be the ones for the Phase Locked Loop control with a damping ratio of $\xi_{PLL} = 0{,}707$.

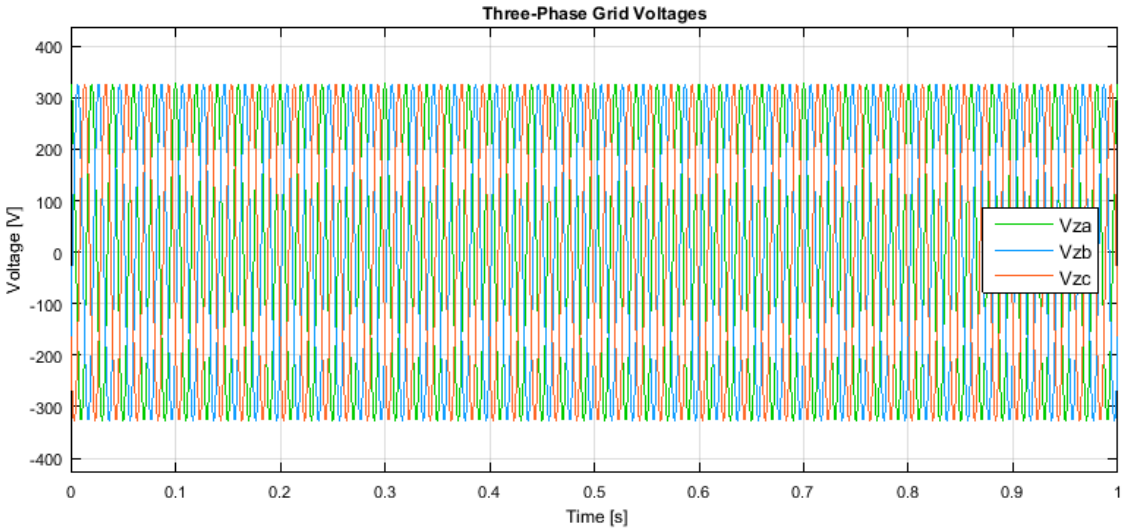

Figure 8.2 Grid voltages in the abc reference frame.

8.1.2. Load parameters

The load simulating the electrical demand as explained in section 6.3 will consist in a constant load consuming 32 kW during the simulation time (1 second).The choice of this value is random and with the purpose of to be able to select a rounded resistance value of exactly 5 Ω. The load could be think of a small local factory with machines consuming a total of 32 kW constantly. This calculus comes from applying Ohm's law (equation (8.2)), the instantaneous power theory (equation (8.3)) and noting that resistances' voltages are equal to the AC grid voltages, thus, applying Park transformation expression (8.1) is obtained. Last note also leads to assume $V_{Ld} = 0$, then, the desired load value is computed (8.4).

$$V_{Lq} = E_m \tag{8.1}$$

$$V_{Lq} = R_L I_{Lq} \tag{8.2}$$

$$P_L = \frac{3}{2}\left(V_{Lq}I_{Lq} + V_{Ld}I_{Ld}\right) \tag{8.3}$$

$$P_L = \frac{3}{2}V_{Lq}I_{Lq} = \frac{3}{2}V_{Lq}\frac{V_{Lq}}{R_L} = \frac{3}{2}\frac{E_m^2}{R_L} = \frac{3\cdot\left(\frac{400\sqrt{2}}{\sqrt{3}}\right)^2}{2\cdot 5} = 32000\ W \tag{8.4}$$

8.1.3. PV system parameters

Firstly, the physical parameters of the system such as the sizing and distribution of the PV modules and the components from the VSC will be presented. Secondly, control parameters will be described.

8.1.3.1. PV physical parameters

Most of the parameters and characteristics of the solar cell used are already described in section 6.1 when modelling the PV system, therefore, only the sizing of the PV system, the irradiance and temperature models will be presented in this case.

For the sizing, supposing that the voltage and current at maximum power of one solar panel from the model chosen is $Vmpp = 40{,}5\ V$ and $Impp = 6{,}05\ A$ [22], then, applying expression (8.5) and taking into account some facts such as the light intensity will change during the simulation, the presence of power losses on the microgrid and in order to be able to distribute the PV modules as rounded numbers (i.e., $N_{modules} = NsNp$), the number of modules implemented will be 144. Note that the power generated by the PV system at MPP will actually be lower than the required by the load.

$$P_{Load} \approx (Ns \cdot Vmpp) \cdot (Np \cdot Impp) \tag{8.5}$$

These 144 modules will be distributed as follow: 7 legs of 18 modules connected in series. That determines the number of modules connected in series (8.6) and number of legs connected in parallel (8.7).

$$Ns = 18 \tag{8.6}$$

$$Np = 7 \tag{8.7}$$

The number chosen for the PV arrays connected in series is due to the common DC bus voltage operates around 800 V because of the AC voltages (400 V).

The irradiance or light intensity (G) profile will change according to Figure 8.3. As mentioned, starting from 9 am (0 second) to 7 pm (1 second), the light intensity increases until 11 am (0.2 second) and then at 2 pm (0.5 second) it decreases. The values taken are inspired by the real irradiance [23], however, it should rise up and decrease gradually and not suddenly as it has been

considered. It is easier to observe the behaviour of the system that way.

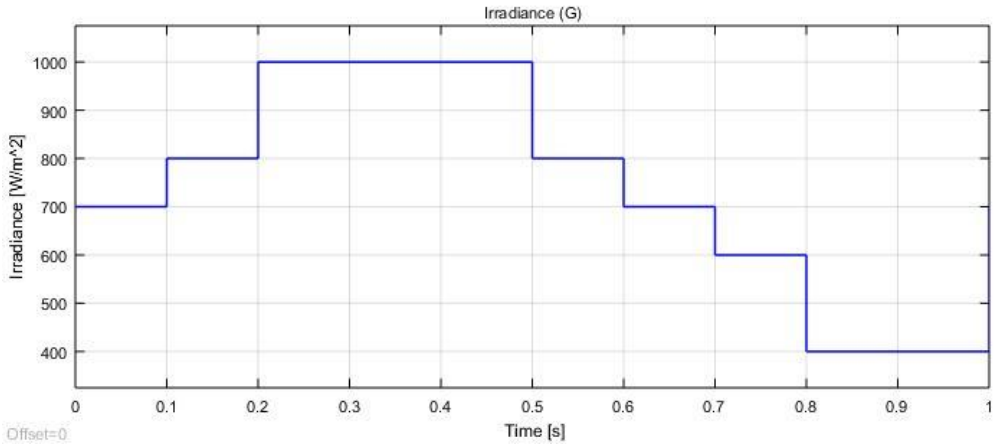

Figure 8.3 Light intensity evolution during the simulation

Likewise, the temperature (T) profile will change suddenly (as a stair) according to Figure 8.4 for the same reason as for the light intensity. It is considered colder during morning and evening and warmer during midday.

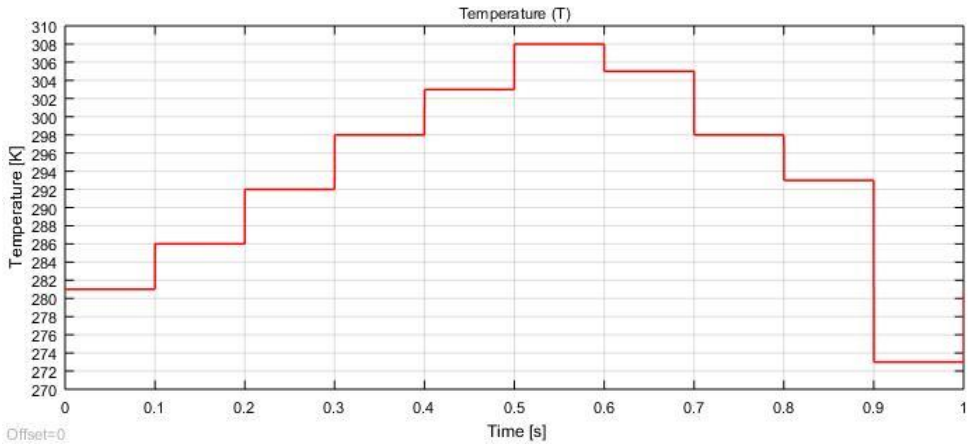

Figure 8.4 Temperature evolution during the simulation

For the VSC converter of the PV system the values for the capacitor are $C = 1020\,\mu F$, the inductance equivalent resistances are $r_l = 0{,}5\,\Omega$ and the inductances values are $l_l = 5{,}4\,mH$ [12].

Finally, the reactive power set points are shown in Figure 8.5.

8.1.3.2. Control parameters

It includes voltage loop parameters and current loop parameters. The angular velocity of the DC voltage loop is set to $\omega_n = 418{,}88\,rad/s$ and damping ratio of $\xi_{DC\_vl} = \sqrt{2}/2$. The time constant of the current loop is $\tau_{cl\_PV} = 1\,ms$, 15 times faster than the voltage loop as recommended for cascaded controllers, these values are taken from [12].

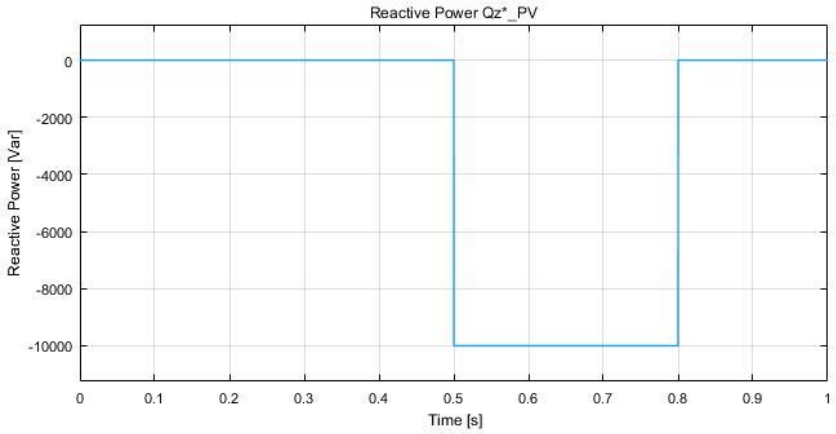

Figure 8.5 Desired reactive power injected to the grid by the PV system.

8.1.4. Battery system parameters

8.1.4.1. Battery physical parameters

Only the voltage between the terminals of the battery is selected due to it has been modelled as a controllable voltage source. Hence the value is set up to $E_{DC\_B} = 800$ V, that is according to the power range that the converter is operating on.

For the VSC converter of the battery system the values for the inductance equivalent resistances are also $r_l = 0{,}5\ \Omega$ and the inductances values are $l_l = 5{,}4\ mH$.

The active power reference values will depend on the function of the battery and will be described for each simulation.

The reactive power reference will change according to Figure 8.6.

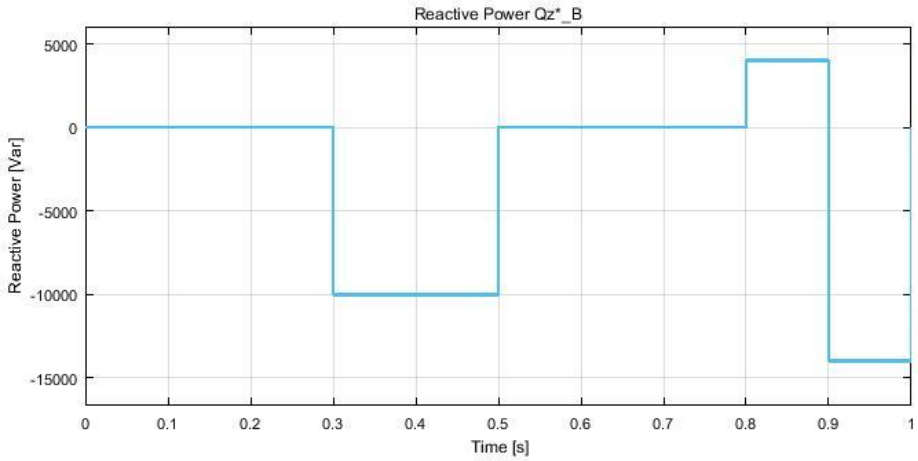

Figure 8.6 Desired reactive power injected to the grid by the storage system.

8.1.4.2. Control parameters

The current loop controllers' time constant for the battery system is $\tau_{cl\_B} = 10\ ms$ [12].

8.2. Simulations

Many simulation have been performed during the elaboration of the study, however, not all of them will be presented due to most of them are small parts from the global system, in other words, the simulations were carried out first system by system and then, all the systems coupled to form the microgrid.

First simulation presented will test the behaviour of the microgrid using the parameters described in the above section and with the storage system operating to generate or consume an active power governed by a superior energy management system.

Second simulation will also test the behaviour of the microgrid using the same parameters, however, in that case, the storage system will operate to support the PV system, i.e. active power reference to the battery system will be the difference between the generated power by the PV system and the consumed power by the load.

Third simulation will be subdivided in two simulations: one for the PV system and one for the battery system, both of them using the VSC real model i.e. using IGBT.

8.2.1. Microgrid general operation

As mentioned, the storage system for this simulation will inject active power to the grid or it will charge the battery according to the active power reference set points shown in Figure 8.6.

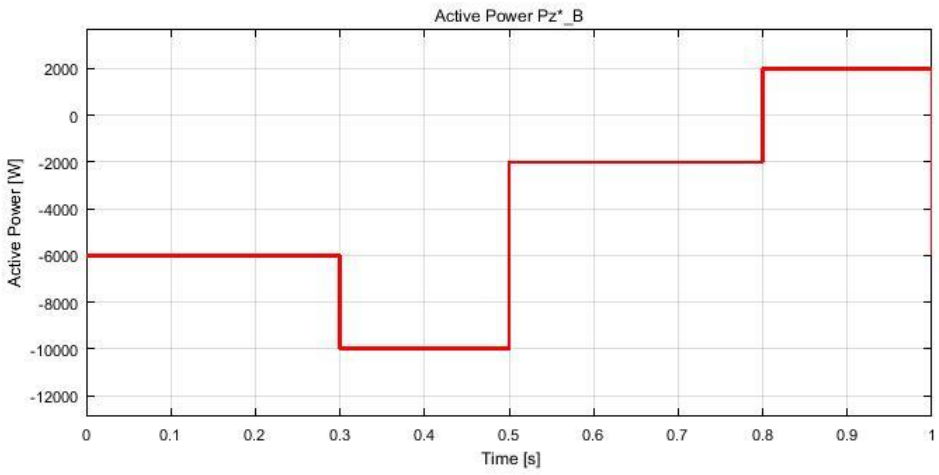

Figure 8.7 Desired active power injected to the grid by the storage system.

Reference and measured values of active power and reactive power of the battery system are illustrated in Figure 8.8. These power values change according to the reference values described before. The power converter can supply reactive power independently of the active power as observed. Negative value of power means that the system is generating power or in other words, the power is injected to the grid, thus, positive value means that the system is consuming power.

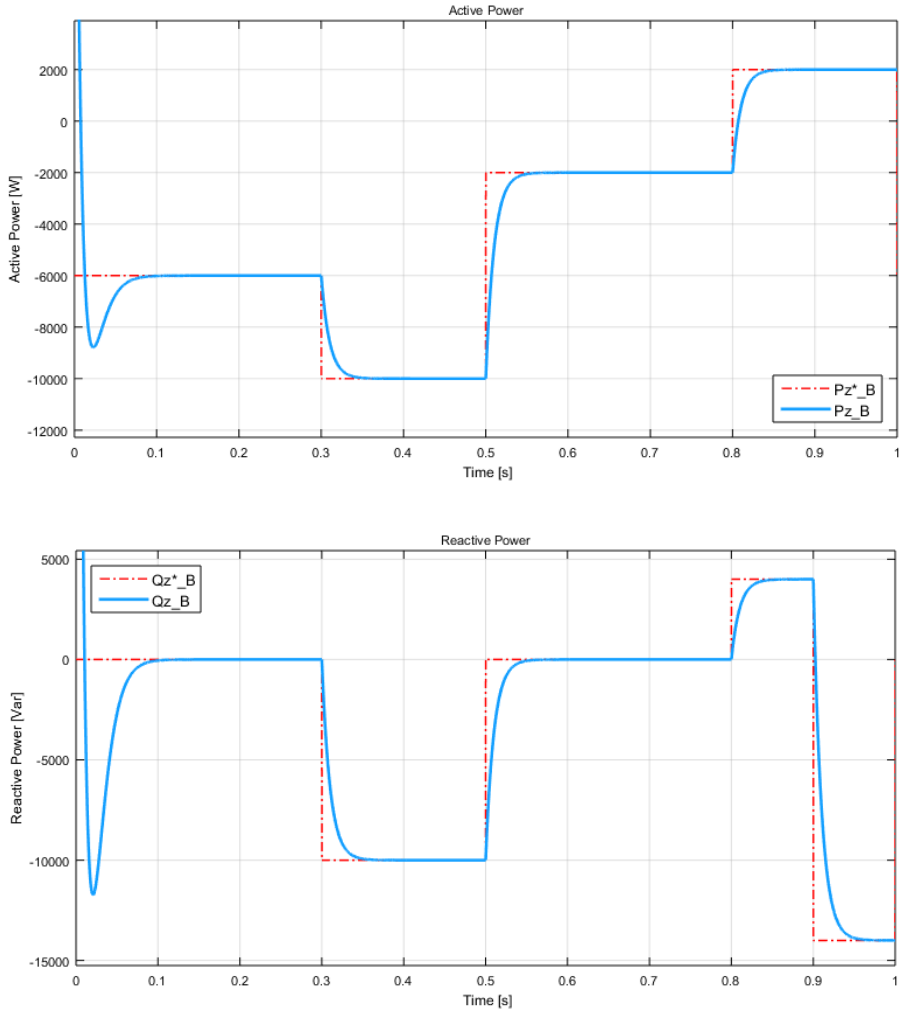

Figure 8.8 Reference and measured active and reactive power Pz_B, Qz_B injected (negative values) to the grid or consumed (positive values) from the grid.

From $t = 0{,}3 - 0{,}5\ s$ and $t = 0{,}9 - 1\ s$ it can be observed in Figure 8.9 that the converter voltages of the battery system increase the magnitude due to the reactive power demand.

A detail of the i_d current evolution is shown in Figure 8.10 to verify that the response of the current loop controller has indeed a time constant of $\tau_{cl\_B} = 10\ ms$ (i.e. for $4\tau_{cl\_B}$ the response reaches 98% of its final value).

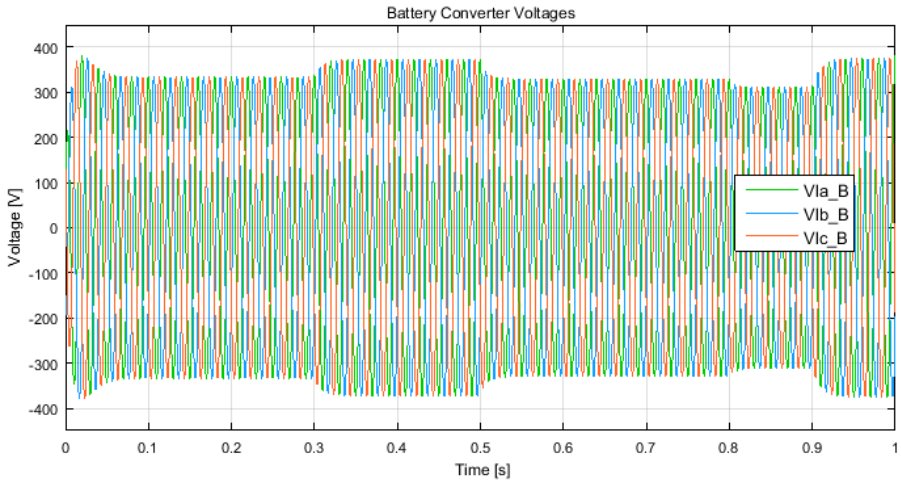

Figure 8.9 Converter voltages from the VSC between the battery and the grid.

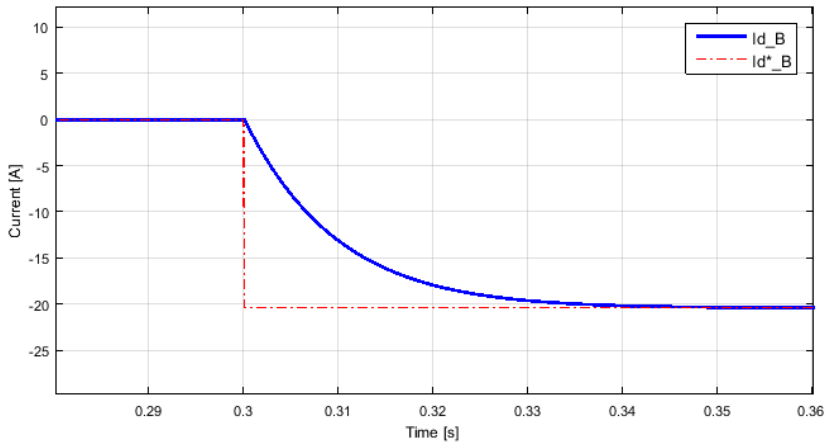

Figure 8.10 Detail of the electrical Id_B response. At τ=10 ms, response reaches 68% of its final value.

In Figure 8.11 it can be seen that the MPPT algorithm is working properly, for the given temperature it computes the voltage at maximum power which is the reference DC bus voltage. The measured DC voltage evolution is also plotted. Each time that DC current changes (Figure 8.13) it takes a few milliseconds to the voltage controller to regulate the bus voltage to the reference value. In Figure 8.12, it can be seen that the DC bus voltage transient behaves accordingly to the control parameters with angular velocity of the system around $\omega_n = 418{,}88\ rad/s$.

Figure 8.13 shows the DC current that the solar PV modules generates and it can be observed that more light intensity means higher light generated current (negative value of current means the PV system is injecting power). It is also observable that from $t = 0{,}2\ s$ to $t = 0{,}5\ s$ where the irradiance is constant, the light generated current increases slightly from $t = 0{,}3\ s$ to $t = 0{,}4\ s$ and from $t = 0{,}4\ s$ to $t = 0{,}5\ s$ due to temperature increment, verifying what it was already seen in chapter 6.

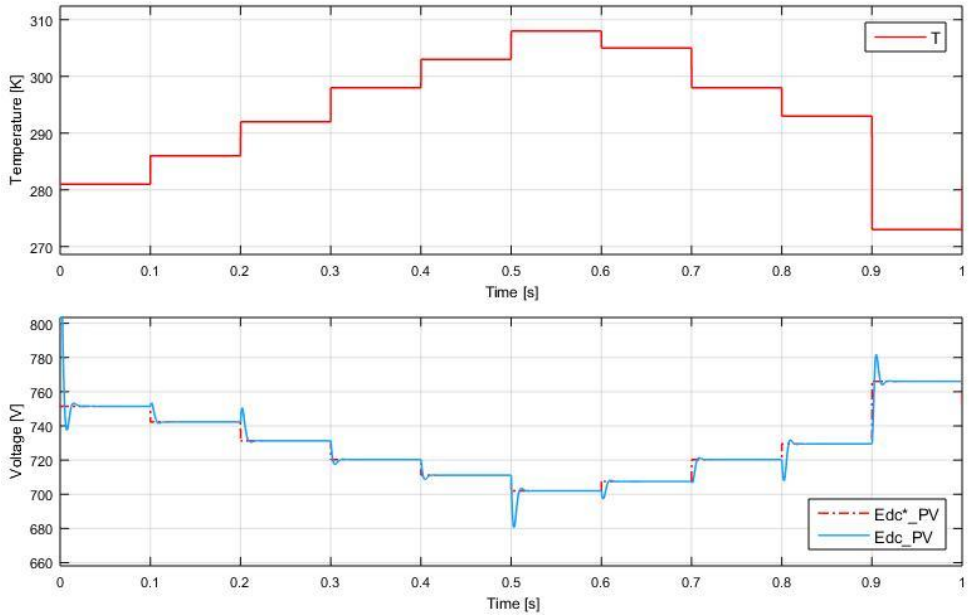

Figure 8.11 Upper graph is temperature vs time. Lower graph is the reference and measured DC bus voltages. As observed, the reference bus voltage which is the output of the MPPT block decreases as temperature increases, satisfying the characteristic of solar modules already seen in chapter 6 (Figure 6.4).

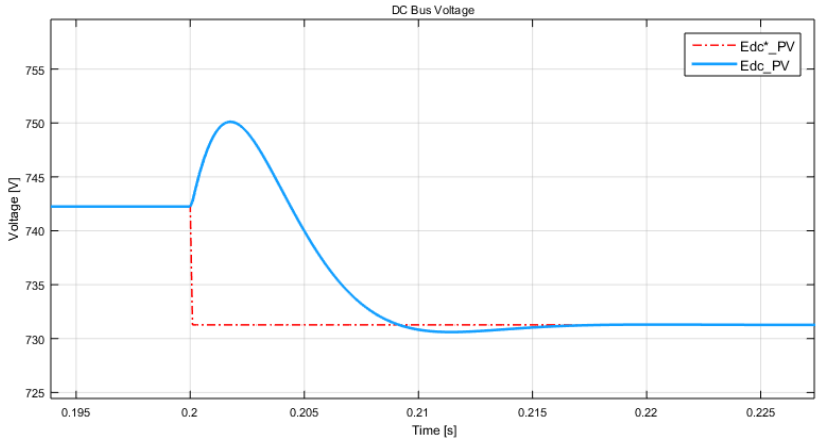

Figure 8.12 Detail of the measured DC bus voltage transient response.

Figure 8.14 shows the evolution of the PV system VSC AC current in the qd and abc references frames. Current Iq_PV changes each time that DC current changes according to Figure 8.13, however, note that it changes inversely due to it is –Idcm instead of Idcm. Likewise, current Id_PV changes according to reactive power reference as shown in Figure 8.5.

The converter voltages of the PV system in the abc reference can be observed in Figure 8.16, the power converter voltage increases when the system injects reactive power between $t = 0{,}5\ s$ and $t = 0{,}8\ s$.

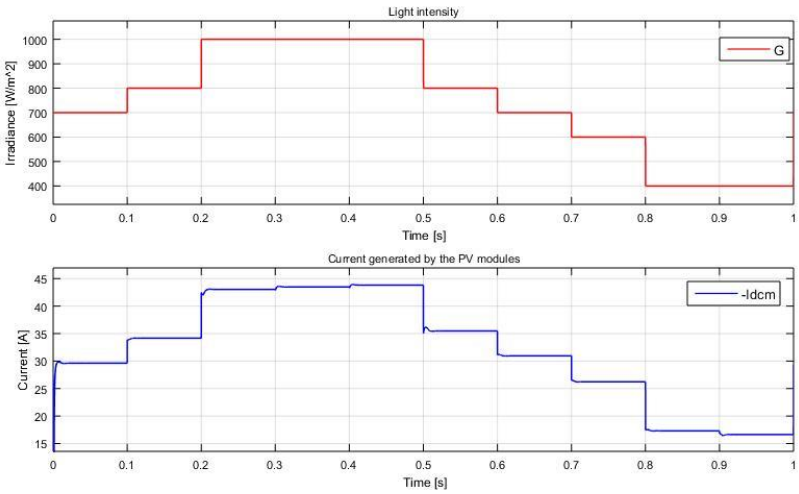

Figure 8.13 Upper graph shows irradiance vs time. Lower graph shows the light generated current by the PV system increasing and decreasing according to light intensity.

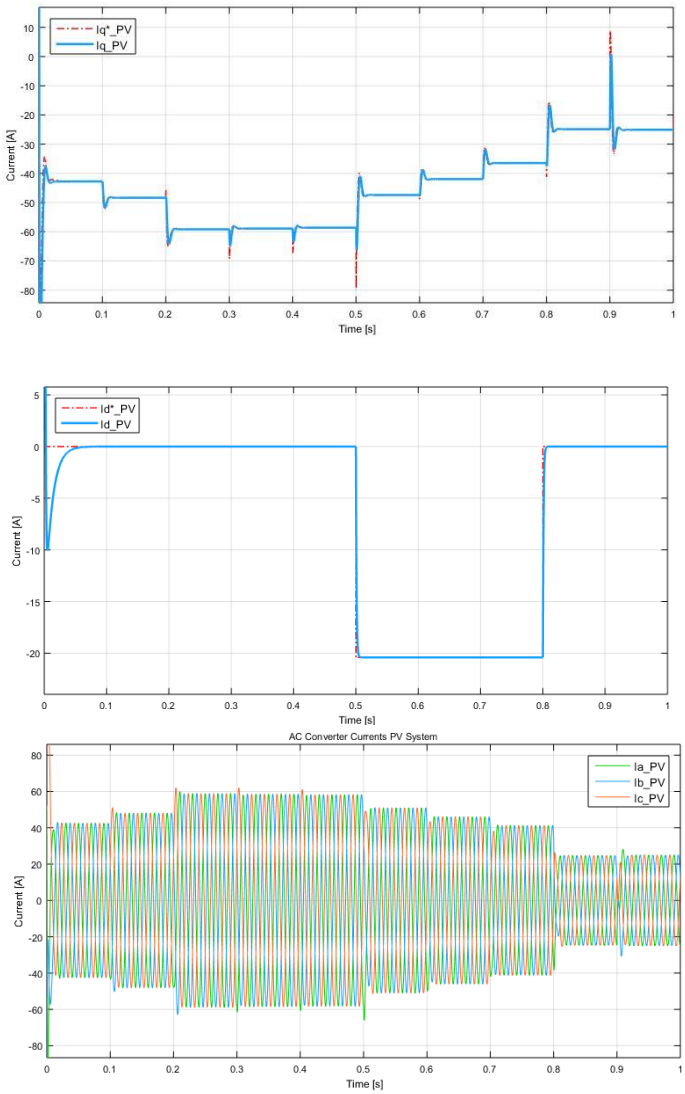

Figure 8.14 Measured and reference currents in the abc and qd reference frame from the PV system.

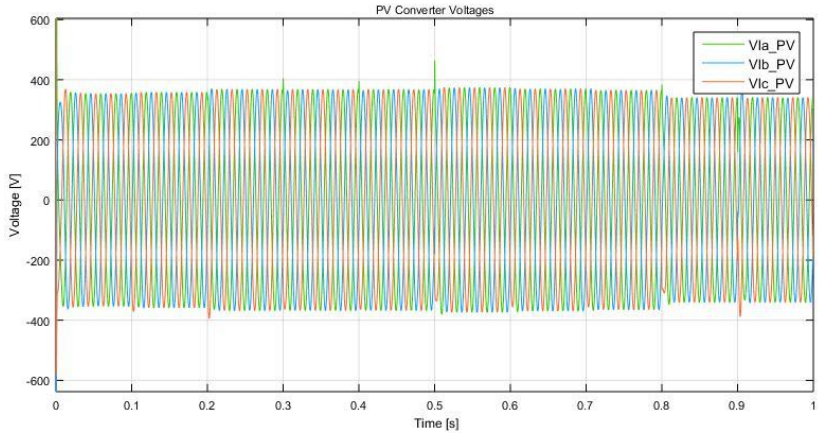

Figure 8.15 PV converter voltages in the *abc* reference frame.

Applying Kirchhoff's current law to the microgrid shown in Figure 8.1 above, it is simple to find expression (8.8). Figure 8.16 shows the evolution of the various currents and it can be checked that the currents satisfy Kirchhoff's law.

$$I_q = I_{q\_L} + I_{q\_B} + I_{q\_PV} \tag{8.8}$$

Where:

$I_q = grid\ current\ in\ the\ qd\ reference$

$I_{q\_L} = AC\ side\ load\ current\ in\ the\ qd\ reference$

$I_{q\_B} = AC\ side\ battery\ current\ in\ the\ qd\ reference$

$I_{q\_PV} = AC\ side\ PV\ system\ current\ in\ the\ qd\ reference$

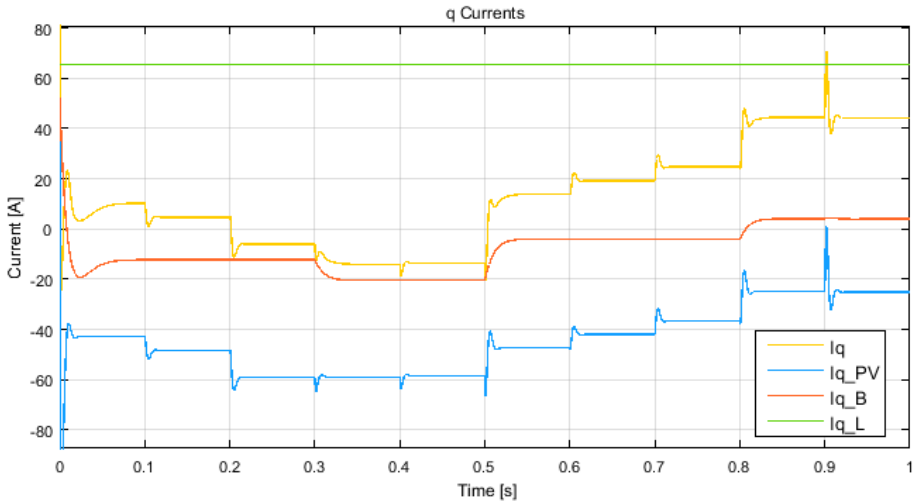

Figure 8.16 Evolution of the Iq currents during the simulation of the microgrid operation.

To avoid any confusion due to possible wrong interpretation, positive values for Iq grid current

means that the main grid is contributing power to the battery system and PV system to deal with the power demand of the load. Likewise, negative values for Iq grid current means that the main grid is receiving power from the generation sources. Same sign convention applies to the interpretation of power balance right below.

Power balance of the entire microgrid is defined by expression (8.9). The different components of the power balance are obtained by applying expression (8.10). VSC ensure that the active power from the AC side of the PV system and the battery system are equal to their corresponding DC side power (as seen in section 6.2).

$$P_T = P_L + P_B + P_{PV} + P_{losses} \tag{8.9}$$

$$P_n = v_{la\_n} i_{a\_n} + v_{lb\_n} i_{b\_n} + v_{lc\_n} i_{c\_n} \tag{8.10}$$

Where:

$P_T = active\ power\ that\ the\ grid\ consumes\ or\ generates$

$P_L = active\ power\ consumed\ by\ the\ load$

$P_B = active\ power\ transferred\ \ by\ the\ VSC\ of\ the\ battery\ system$

$P_{PV} = active\ power\ transferred\ by\ the\ VSC\ of\ the\ PV\ system$

$P_{losses} = active\ power\ dissipated\ by\ the\ impedances$

$n = T, L, B, PV, losses$

Figure 8.17 shows the active power generated or consumed by the different elements of the global system and the results show that the behaviour of the system is the one expected. Power losses from the inductors and inductances equivalent resistances are not plotted in Figure 8.17 although it can be seen that they exist due to if the plotted power values at a specific time are applied to expression (8.9), a non-zero value is obtained which is the power due to losses of the inductors elements.

From $t = 0{,}2\ s$ to approximately $t = 0{,}5\ s$ the power seen by the main grid (P_{ac_T}) is negative meaning that the microgrid is injecting power to the main grid.

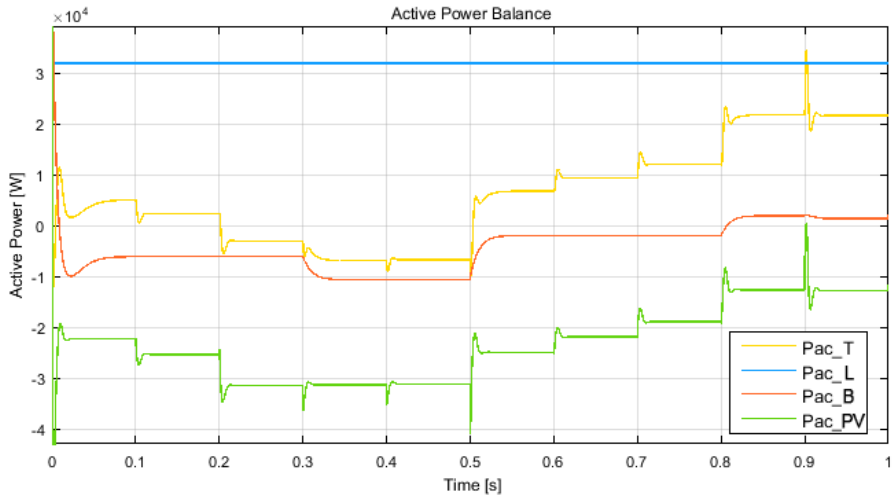

Figure 8.17 Evolution of the active power during the simulation of the microgrid operation.

8.2.2. Battery operating to support the PV system

For this simulation, storage energy will act in order to support the PV system to reach the power required by the load. It could be think of the basis of a stand-alone system, due to the battery active power reference ($P^*_{z\_B}$) will be guided by expression (8.11), i.e. the battery will generate the deficit power that the PV system (P_{PV}) needs to achieve the one demanded by the load (P_L) or it will store the excess energy when the PV system generates more power than required by the load.

$$P^*_{z\_B} = P_{PV} - P_L \tag{8.11}$$

However, as mentioned earlier, the battery has been modelled as a simple voltage source without taking into account the capacity of it neither the state of charge, therefore, it will act ideally.

Another parameter that has been modified is the load with the purpose of making the simulation a bit more interesting, now, the load will consume 20 kW (R_L= 8 Ω) instead of 32 kW. Since all the rest of the parameters have been kept, only the new results will be shown and discussed.

The main difference is at the battery performance and at the main grid. In that case, the main grid should act as if it is not there due to the battery is contributing the rest of the power to deal with the load. Nevertheless, its value is not constantly zero as it can be observed in Figure 8.18 and the reason is the existence of power losses (inductors and its equivalent resistances), not supported by the battery.

Results show that during the daylight (roughly until $t = 0{,}7\ s$ or 4 pm) the PV system is generating enough energy to fulfill the power demanded by the load, thus, the value of the battery power is positive, meaning that it is charging the excess amount of power produced by the PV modules. From $t = 0{,}7\ s$ onwards, the battery is injecting power to the microgrid to support the PV system reach the power requested by the load, hence, the power value is negative.

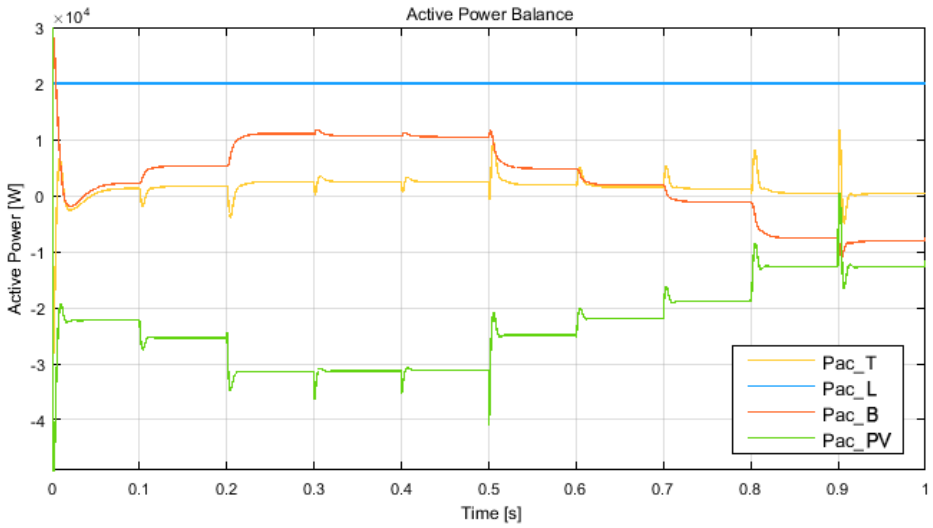

Figure 8.18 Evolution of the active power during the simulation of the microgrid with the storage system supporting the PV system.

8.2.3. Voltage Source Converter real model

The following two simulations apply SPWM technique to modulate the converter voltages into pulses to tell the IGBTs when to switch. Some parameters have been modified to show the behaviour of the system more clear, they will be specified.

To accomplish the few requirements mentioned in the last chapter to design a proper modulation, they are summarized here with the parameters selected:

1) Carrier signal amplitude: it has to be greater than the modulated signal amplitude to satisfy a modulation index lower than 1, which is around $E_m = 400\sqrt{2}/\sqrt{3}\ V$ as observed in the previous simulations, furthermore, none of the converter voltages are above 400 V, therefore this will be the chosen amplitude for the carrier signal, $A_c = 400\ V$.
2) Switching frequency should be at least 10 times faster than the current loop time constant controller. Considering for this case that both battery system and PV system have a $\tau_{cl\_B} = \tau_{cl\_PV} = 1\ ms$, the time constant or period in this case for the switching frequency has to be at least $\tau_{carrier} = 0{,}1\ ms$, or which is equal to 10.000 Hz.
3) Finally, as the project works with three-phase grid, it is recommended that the frequency relation belongs to a multiple of 3 to be able to use only one carrier signal for the three phases. Hence, knowing that modulating signal frequency is 50 Hz and applying expression (7.29), the ultimate values for the switching frequencies are found (8.12).

$$k = \frac{10000\ Hz}{3 \cdot 50\ Hz} = 66{,}67 \approx 67 \ \rightarrow \ f_{carrier\_B} = f_{carrier\_PV} = 67 \cdot 3 \cdot 50\ Hz = 10.050\ Hz \quad (8.12)$$

Likewise, already mentioned in the last chapter, typical values for switching frequency are between 2 – 15 kHz, therefore, the chosen ones also fulfill this characteristic.

In order to reduce the high frequencies noise generated by switching the IGBTs, inductors are applied to act as filters improving the results obtained. These inductors will have a value of $L_2 = 10\ mH$.

A schematic Simulink model for the SPWM block is shown in Figure 8.19. The six outputs are the inputs for each IGBT; however, to avoid any short circuit, a phase can only have one IGBT (out of two) switched on, i.e. both IGBTs per phase will have opposite square form wave of values 1 and 0 as input signal to tell them when to open and when to close.

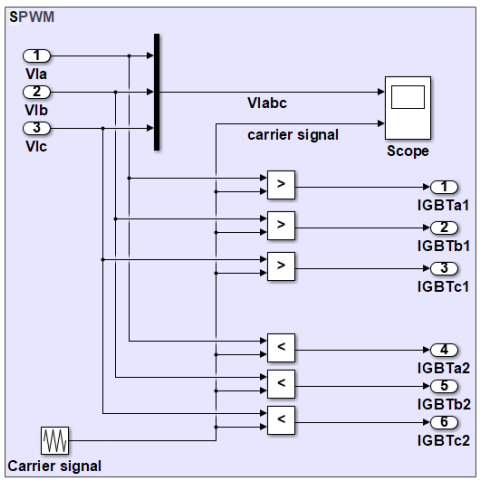

Figure 8.19. Simulink model of the SPWM block applied.

8.2.3.1. VSC using IGBTs on Battery System

A schematic simplified Simulink model of the Battery System connected to the grid is shown in Figure 8.20.

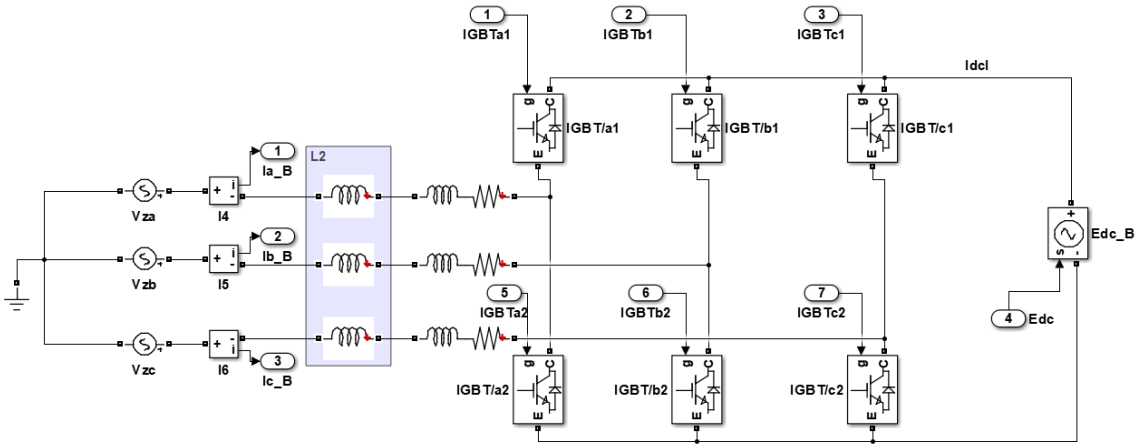

Figure 8.20 Simulink scheme of the VSC real model of the battery system.

For this simulation, the reference active and reactive power are not exactly the same as for the previous simulations. Reference and measured values of active and reactive power are shown in Figure 8.21. The existence of ripple due to switching is observable and the behaviour is the one desired.

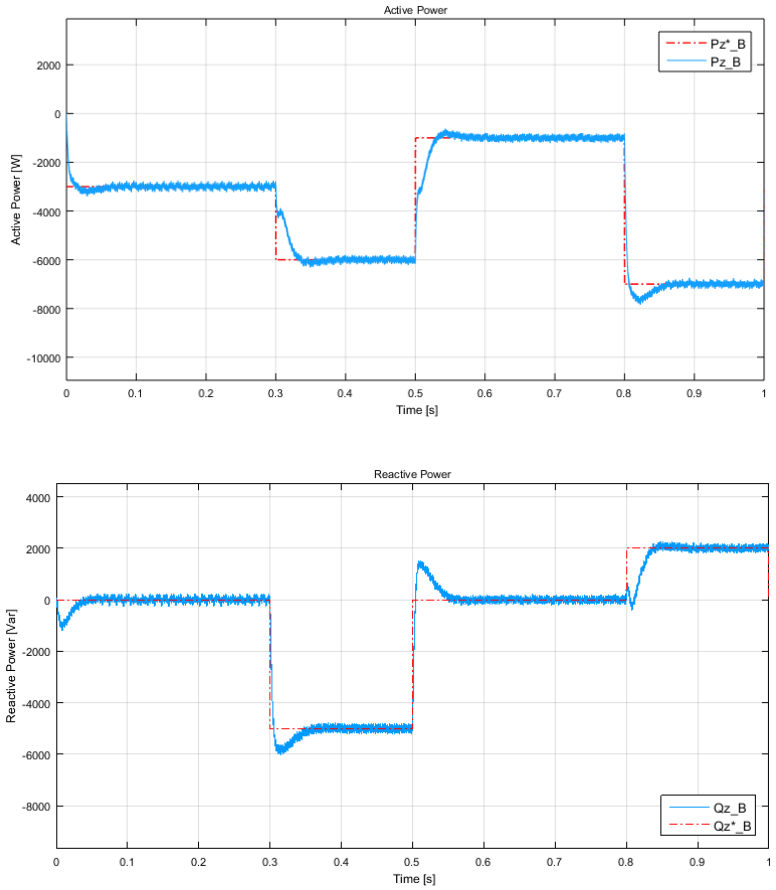

Figure 8.21 Reference and measured values of active power and reactive power during the simulation using VSC real model.

Figure 8.22 shows a detail of the triangular carrier signal vs the modulating signal. Square wave forms signals obtained can be observed in Figure 8.23 from $t = 0{,}218\,s$ to $t = 0{,}222\,s$, compared to the previous Figure 8.22 for the same period of time it can be conclude that the modulation is correct. Likewise, the AC currents in the abc frame are presented in Figure 8.24 and a close detail of the currents are in Figure 8.25. The system behaves as expected and the imperfect sine waves due to switching are visible in the close detail.

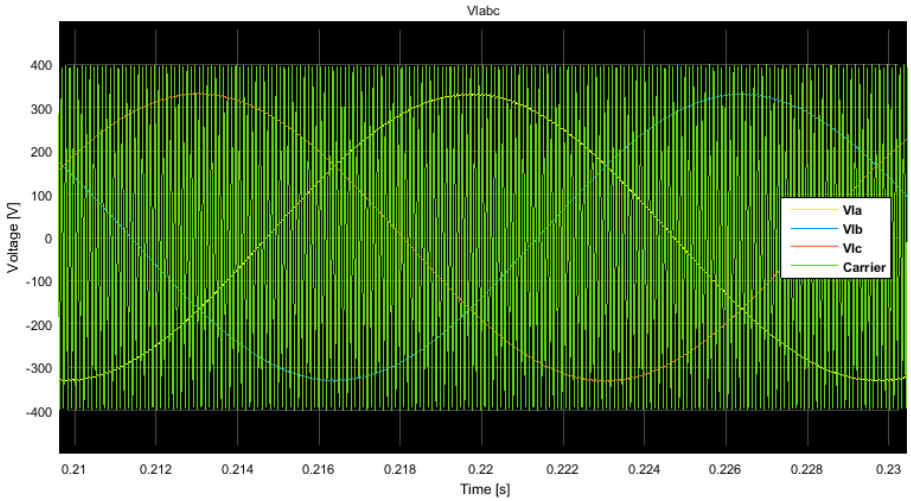

Figure 8.22 Detail of the carrier signal vs the converter voltages.

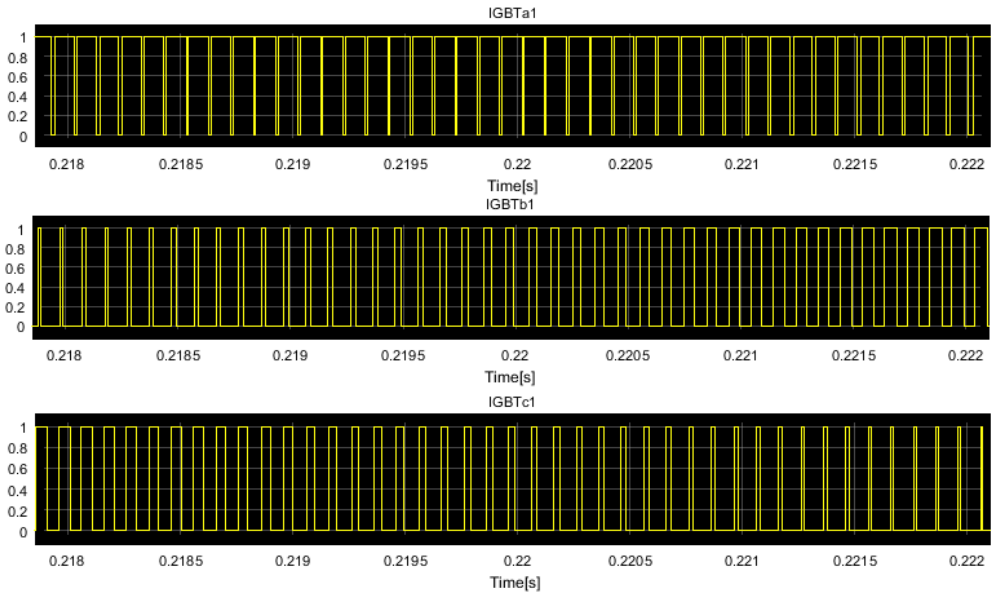

Figure 8.23. Detail of the modulated converter voltages by applying SPWM.

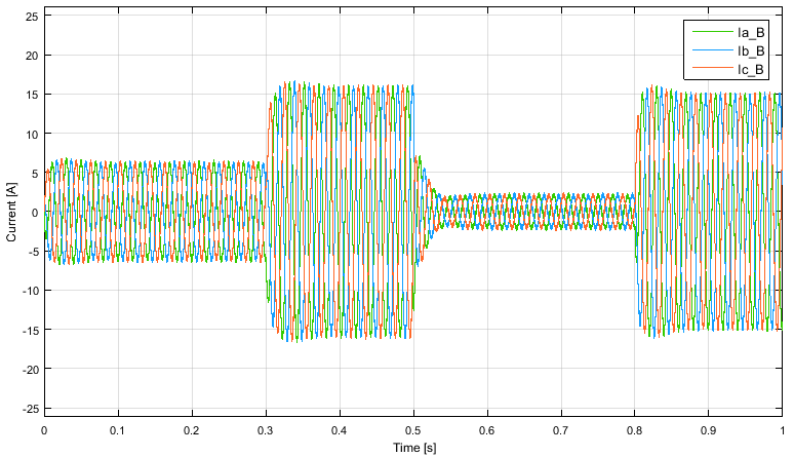

Figure 8.24. Measured currents in the *abc* reference frame using VSC real model.

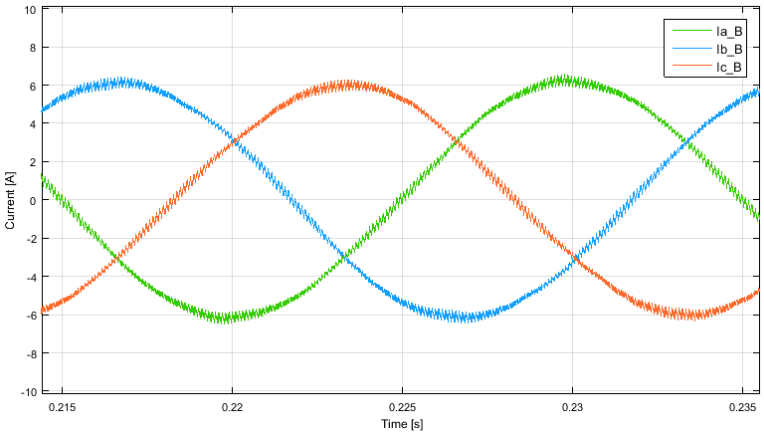

Figure 8.25 Detail of the measured currents in the *abc* reference frame using VSC real model.

8.2.3.2. VSC using IGBTs on PV System

A schematic simplified Simulink model of the PV System connected to the grid is shown in Figure 8.26. In that case, the PV system will be simplified and the power generated is changed by changing the current of the DC source according to Table 8.1 and the DC bus voltage is maintained at 800 V constantly. Reactive power set points are also described in Table 8.1.

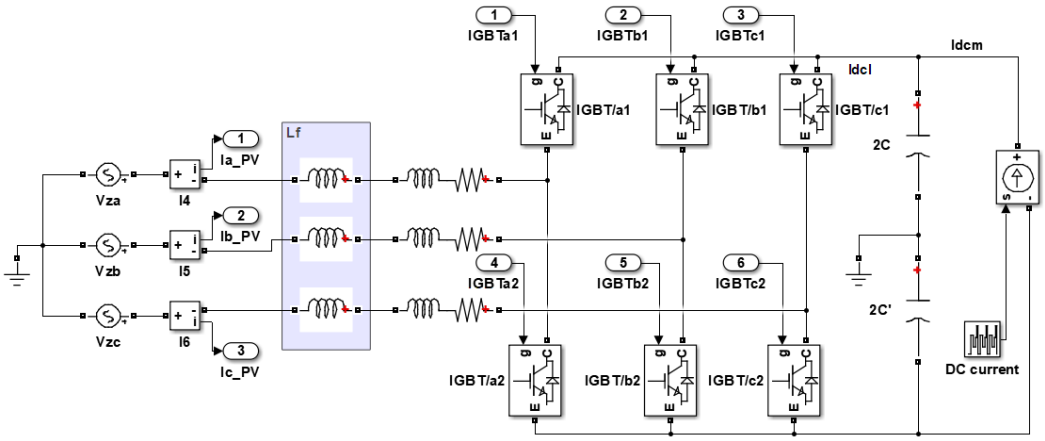

Figure 8.26 Simulink scheme of the VSC real model of the PV system.

Time instant [s]	*DC current [A]*	*Reactive power reference [Var]*
t=0	4	0
t=0,3	9	0
t=0,5	6	-3000
t=0,8	8,5	-3000
t=0,9	11,5	0

Table 8.1 DC current and reactive power reference values for the simulation using VSC real model

Figure 8.27 shows the evolution of the current in the qd and abc reference frames. As expected, both currents Iq and Id change according to Table 8.1 in addition to the small amount of ripple due to switching.

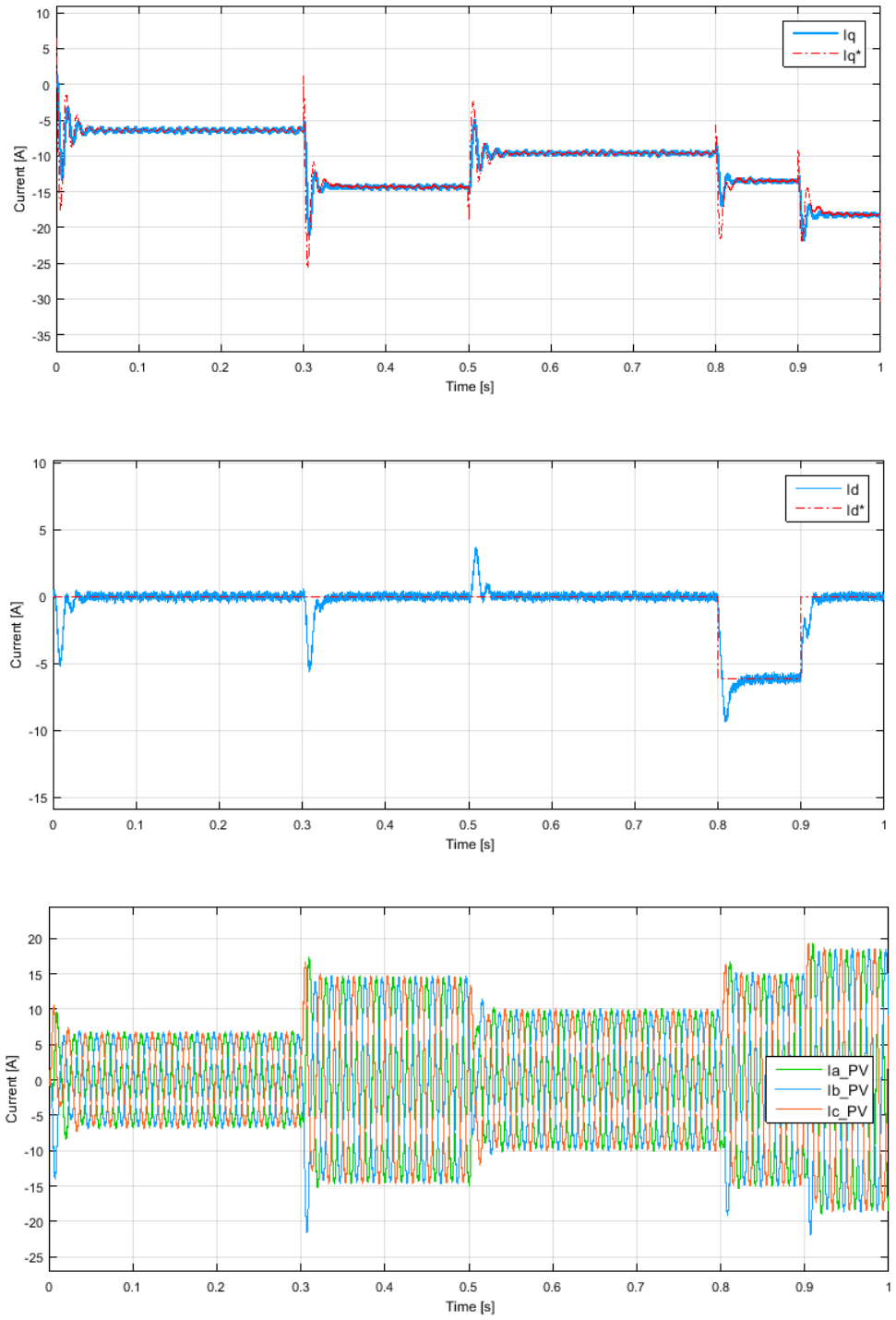

Figure 8.27 Reference and measured currents in the qd and abc frame for the simulation using VSC real model

The DC bus voltage evolution is shown in Figure 8.28. The peak of the measured bus voltage is

higher for larger injected DC currents. The model behaves as expected keeping the DC bus voltage at 800 V. Ripple presence due to switching is also visible here.

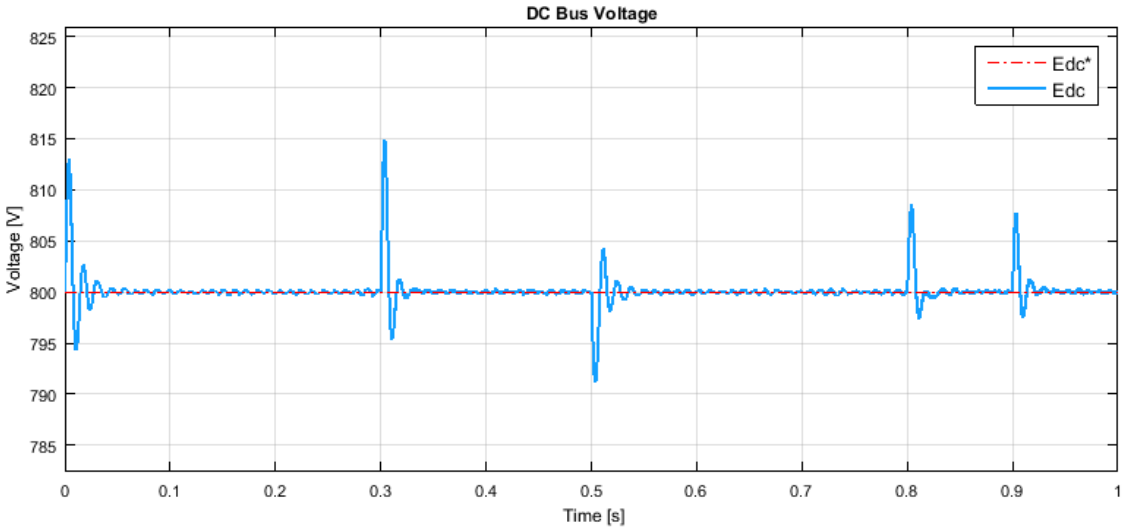

Figure 8.28 Evolution of the DC bus voltage for the simulation using VSC real model.

9. Budget

An approximation of the cost to elaborate this project will be presented in this chapter. It will contain the cost for the human resources employed and also the cost of material resources to make this study.

A budget in case of implementing physically the microgrid is not evaluated due to it could be considered as another entire project: to analyse the economic viability of implementing it, to optimize it making a full study of the geographical location, weather conditions, inverters and battery capacity and so on.

9.1. Study cost

As mentioned it includes the workload as well as the equipment used to make the study.

9.1.1. Human resources

This item considers the hours spent to elaborate the project. This time is divided in the following sub items.

- Investigation: it includes the hours dedicated to search information about the topic and theoretical background.
- Study, design and modelling: it covers the time spent to design the microgrid, to study its elements and to model it. It also covers the mastering of the software used.
- Simulations: it adds the hours put in to verify the model by simulating it with Simulink and analysing the results applying the knowledge acquired previously.
- Writing: it shows the hours dedicated to write the memory of the project.

The budget of this item is shown in Table 9.1. The price per hour taken is the value that the author of the project considers fair for a recently graduated engineer.

Sub Item	Price [€/hour]	Hours [hour]	Total [€]
Investigation	20,00	50	1.000,00
Study, design and modelling	20,00	225	4.500,00
Simulations	20,00	150	3.000,00
Writing	20,00	105	2.100,00
Subtotal	20,00	530	**10.600,00**

Table 9.1 Human resources cost

9.1.2. Material Resources

This item includes all the equipment, software tools and transport tickets to the university used to make this study. For the equipment, an amortized cost period of six months, which is the duration of the project, has been considered. The breakdown of expenses are shown in Table 9.2.

Equipment				
Sub item	**Price per unit [€]**	**Quantity**	**Lifecycle [years]**	**Total Amortized [€]**
Laptop	500,00	1	7	35,71
Peripheral- Mouse	10,00	1	4	1,25
Software and Transport				
Sub item	**Price per unit [€]**	**Quantity**		**Total [€]**
MATLAB R2015a with SymPower Systems	119,00	1		119,00
T-Jove Trimestre (3 zones)	199,20	2		398,40
Subtotal				**556,36**

Table 9.2 Material Resources cost

9.1.3. Total cost

Both items are added up and the taxes are applied to obtain the budget of the entire project (Table 9.3).

Item	**Total [€]**
Human Resources	10.600,00
Material Resources	556,36
Subtotal	11.156,36
Total (21% IVA)	**13.499,20**

Table 9.3 Total cost of the project

10. Environmental Impact Assessment

Although the scope of the project does not include the implementation of the designed microgrid, an environmental impact assessment will be presented in this chapter in case of implementing it, due to the obvious fact that the present study itself does not have an important environmental impact, a part from the electricity used to carry out all the simulations.

One of the benefits of microgrids are that they integrate renewable energy sources, in that case, solar energy, which help to minimize carbon footprint and greenhouse gas emissions. However, solar energy are not a free emission source. The manufacturing of solar modules, the obtaining process of raw material such as silicon, especially high purity silicon, all of them consume a big amount of energy, and not precisely from renewable sources [24]. All these emissions are called indirect emissions and most of the manufacturers when making a product they elaborate its Environmental Product Declaration (EPD) due to it considers the indirect emissions through the life-cycle of the product. Life-cycle analysis (LCA) are regulated by the ISO 14040 norms.

LCA is a technique to assess environmental impacts associated with all the stages of a product's life from raw material extraction through materials processing, use, disposal or recycling.

Nevertheless, environmental impact assessment is an assessment of the possible positive or negative impact that a proposed project may have on the environment, considering ecosystem, social and economic aspects.

The following sections evaluates the design considerations and the impact during the implementation of the microgrid.

10.1. Design evaluation

In order to minimize the negative impact that the designed microgrid may have on the environment it is fundamental to obey and follow the laws, norms and directives.

For instance, all the components belonging to the PV system, battery system and inverters, must follow the Directive 2012/19/EU about waste electrical and electronic equipment, due to many of the components from a solar module or battery could be hazardous if the disposal or recycling are not correctly done. Likewise, the Directive 2011/65/EU regarding to the restriction of the use of certain hazardous substances in electrical and electronic equipment is essential for the manufacturing of solar arrays and batteries.

The PV system designed is intended to be built on the small factory roof, therefore, it will have minimal land use and visual impact [24].

Noise from the components (especially converters) of the microgrid have also minimal impact to the environment due to they are usually placed in areas not too close to the population.

Managing electrical components may have a risk of producing fires, it is important to follow the installation regulation of protection against fires of the country where the microgrid could be implemented.

No negative impact to the ecosystem should be made due to it is intended to be built on the roof of a factory; therefore, the factory was already there before with the corresponding fauna and flora of the chosen location.

10.2. Impact during the implementation

As the microgrid is a relatively small scale installation, the negative impact during the installation phase and operation phase are primarily due to transportation of the 144 solar PV modules to the factory location.

However, the lifetime of the batteries are shorter than of the PV modules [25], for this reason, the changing and disposal of the battery bank used will have an impact or another depending on the kind of battery used. For instance, lithium ion batteries have a greater cycle life and are cleaner technology than lead acid batteries, therefore, lithium ion batteries have less environmental impact than the lead acid ones [26].

Lifespan of photovoltaic modules are around 25 years. The dismantling phase of the PV system is not laborious and it does not affect the land where it was, however, the disposal and recycling of its elements have the greatest impact. Contacting with the manufacturers could give an idea of what is the best option, due to nowadays, companies receive incentives if they recycle their own products or high valuable often rare products that a solar PV module could probably contain [24].

11. Conclusions

The present project has studied step by step the design, modelling, control and simulation of a microgrid based on several elements with special focus to the photovoltaic system and to the voltage source converters. The remainder elements composing the microgrid, the storage system and the load, have been briefly introduced and represented without any complexity.

Modelling of the equivalent electric circuit to simulate the working principle of a photovoltaic cell has been presented in detail, satisfying all its properties. A maximum power point tracking (MPPT) control algorithm in order to force the PV system work at its best performance point has been explained and applied. A complete review of the VSC simplified model has been elaborated and successfully implemented to connect both DC sources (PV system and battery storage system) to the main AC three-phase grid. Likewise, a pair of examples using the real model of the VSC based on six IGBTs have been tested all implementing Sinusoidal Pulse Width Modulation (SPWM) to control the opening and closing of them with positive results.

The good behaviour of the entire microgrid has been verified using Matlab Simulink, power balances and current balances are according to the given parameters, and the correct control methodology ensures that a change in one of the components of the system disturbs other components in order to reach a new balanced state in a small amount of time, defined by the designed controllers.

While designing the presented microgrid, one realizes that its flexibility allows to implement any other design besides the one studied due to its elements have been previously built and tested separately. For instance, the size of the PV system could be extended just changing the number of modules connected, a second storage system could be applied or an extra load could be added to the microgrid without the need to start all the design neither the control from scratch.

Finally, potential future works proceeding the presented one will be briefly described in the following section. Some are improvements of the current microgrid and others are simply future line works about aspects that the present work has not covered.

11.1. Future works

One possible line to follow would be to improve the studied microgrid by minimizing the initial transient peak amplitude at time 0.0 s observed in all the simulations. Likewise, to apply the VSC real model to the entire microgrid and to try other PWM methods, for example Space Vector Pulse Width Modulation, in order to make a comparison to determine which method is the most suitable for several scenarios.

Another possible line work would be modelling the energy storage system to be more realistic, i.e. the battery system with all its characteristics such as the capacity, state of charge, depth of discharge among others. This would also mean to adjust the simulation time to the reality or to adjust the parameters of the system to the simulation time. Same would apply to the load modelling or even better, a complete study of the energy management system to distribute the power each element of the microgrid generates or consumes in order to make the grid perform at its highest efficiency.

Third suggestion would be to add other renewable generation sources to the microgrid and/or to make a complete study of the economic and technical viability in case of implementing the microgrid in a specific location, taking into account the laws, costs, licenses and other requirements of the chosen country.

Last proposal is to check that the microgrid fulfill with the grid code requirements. For instance, fault ride-trough requirement, voltage support, ramp rate or frequency support among others. Some of them might need additional equipment such as energy storage systems to satisfy the requirements and controllers to manage them.

Acknowledgements

I would like to thank the department of CITCEA for the help I received from them on the making of this project as well as the director of the project to introduce me this topic where I could enhance my knowledge on Solar Photovoltaic and broaden my knowledge about converters.

I also appreciate all the support my family and friends gave to me during the elaboration of this project.

References

[1] ENGIE. *Microgrids: descentralized energy*. [https://www.engie.com/en/businesses/microgrids-decentralized-energy/, 17th January 2018]

[2] EUROPEAN COMISSION. *Renewable energy.* [https://ec.europa.eu/energy/en/topics/renewable-energy, 20th December 2017]

[3] REN21. *Renewables 2016 Global Status* Report. Paris: REN21 Secretariat, 2016.

[4] WESSOF, E. *IEA: Global installed PV Capacity Leaps to 303 Gigawatts.* Green Tech Media. April 2017. [https://www.greentechmedia.com/articles/read/iea-global-installed-pv-capacity-leaps-to-303-gw#gs.yisqIQ8, 20th December 2017]

[5] INTERNATIONAL ENERGY AGENCY. *2016 Snapshot of Global Photovoltaic Markets*. 2017

[6] WORLD ENERGY COUNCIL. *World Energy Resources 2013 Survey.* England and Wales: 2013.

[7] TSAGAS, I. *Spain Approves 'Sun Tax', Discriminates Against Solar PV*. Renewable Energy World. October 2015. [http://www.renewableenergyworld.com/articles/2015/10/spain-approves-sun-tax-discriminates-against-solar-pv.html,20th December 2017]

[8] ENERGYX: SUSTAINABLE ENERGY: DESIGN A RENEWABLE FUTURE. *How does a PV cell work? – Sustainable Energy – TU Delft*. Delft: 2016. [Video]

[9] WIKIMEDIA. *Solar Cell IV graph.* [https://upload.wikimedia.org/wikipedia/commons/8/8d/SolarCell-IVgraph3-E.PNG,11th November 2017]

[10] PV EDUCATION. *Effect of parasitic Resistances.* /http://www.pveducation.org/pvcdrom/effect-of-parasitic-resistances, 11th November 2017]

[11] ENERGYX: SUSTAINABLE ENERGY: DESIGN A RENEWABLE FUTURE. *How does an inverter and MPPT of a PV system Work? – Sustainable Energy – TU Delft*. Delft: 2016. [Video]

[12] EGEA, A., JUNYENT, A., GOMIS, O. *Active and Reactive Power Control of Grid Connected Distributed Generation Systems.* Green Energy and Technology. Heidelberg: 2011, pp 47-81.

[13] GENERAL MICROGRIDS. *What is a microgrid?* [https://www.generalmicrogrids.com/about-microgrids, 28th December 2017]

[14] WALKER, G. *Evaluating MPPT Converter Topologies using a Matlab PV Model.* University of Queensland. Australia: 2001.

[15] DÍAZ, F., SUMPER, A., GOMIS, O. *Energy Storage in Power Systems*. John Wiley & Sons, 2016.

[16] FREEMAN, D. *Introduction to Photovoltaic Systems Maximum Power Point Tracking.* Texas Instruments. November 2010.

[17] MATHWORKS. *Implement maximum power point tracking algorithms for photovoltaic systems using MATLAB and Simulink.* [https://es.mathworks.com/discovery/mppt-algorithm.html, 16th December 2017]

[18] MATHWORKS. *Documentation PV Array.* [https://www.mathworks.com/help/physmod/sps/powersys/ref/pvarray.html, 20th December 2017]

[19] CHUNG,S.-K. *A phase tracking System for three phase utility interface inverters*. IEEE Transactions on Power Electronics. 2000. Vol 15, pp. 431-438.

[20] HARNEFORS, L., NEE, H.-P. *Model-based current control of ac machines using the internal model control method*. IEEE Transactions on Industry Applications. 1998. Vol 34(1), pp.133–141.

[21] GOLE, A.M. *Sinusoidal Pulse width modulation*. 2000. pp. 1-8

[22] SUNPOWER. *E19/245 Solar Panel Datasheet.* [https://us.sunpower.com/sites/sunpower/files/media-library/data-sheets/ds-e19-series-245-solar-panel-datasheet.pdf, 15th October 2017]

[23] EUROPEAN COMISSION JRC. *PVGIS*. [http://re.jrc.ec.europa.eu/pvgis/apps4/pvest.php?lang=es&map=Europe, 19th December 2017]

[24] UNION OF CONCERNED SCIENTISTS. *Environmental Impacts of Solar Power.* March 2013. [https://www.ucsusa.org/clean_energy/our-energy-choices/renewable-energy/environmental-impacts-solar-power.html#.WlJlgN_ibIU, 7th January 2018]

[25] ENERGYX: SUSTAINABLE ENERGY: DESIGN A RENEWABLE FUTURE. *Central design rules for PV systems – Sustainable Energy – TU Delft*. Delft: 2016. [Video]

[26] MESSINA, C. *7 Facts Comparing Lithium-ion with Lead Acid Batteries.* Relion. August 2015. [http://www.relionbattery.com/blog/7-facts-and-figures-comparing-lithium-ion-vs.-lead-acid-batteries, 7th January 2018]

[27] PARK, R.H. *Two-reaction theory of synchronous machines.* AIEE Transactions. 1929. Vol. 48, pp. 716-730.

[28] AKAGI, H., KANAZAWA, Y., NABAE, A. *Generalized theory of the instantaneous reactive power in three-phase circuits*. International Power Electronics Conference. 1983. pp. 1375-1386.

[29] AKAGI, H., WATANABE, E., AREDES, M. *Instantaneous power theory and Applications to power conditioning*. Wiley, Chichester. 2007

Appendix A

Park Transformation

Park transformation was first proposed by Robert H. Park in 1929 [27]. It is a mathematic transformation used nowadays to simplify the analysis and study of electrical three phase systems due to the oscillating nature of those systems when working with AC makes them not really convenient. For instance, for the controller design it is useful to have constant quantities, hence, applying the Park transformation it is possible to achieve constant values instead of oscillating values.

Also known as $dq0$ transformation, it can be thought as the projection of the three phase (abc) quantities onto a rotating two-axis reference frame (Figure A.1). In other words, given a vector in abc reference frame (x_{abc}), when applying Park Transformation, the same vector in $qd0$ reference (x_{qd0}) will be obtained (A.1).

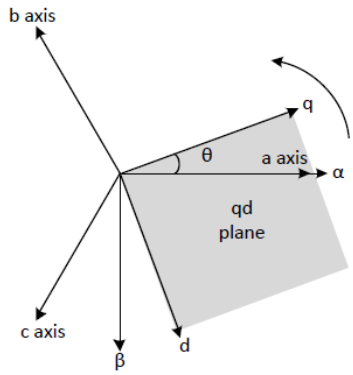

Figure A.1 dq plane representation. Source: [12]

$$[x_{qd0}] = [T_{qd0}][x_{abc}] \tag{A.1}$$

There exists many transformations matrix forms of the Park Transformation concept, the one used for this project is shown in (A.2) and its inverse is shown in (A.3).

$$T(\theta) = \frac{2}{3}\begin{bmatrix} \cos(\theta) & \cos\left(\theta - \frac{2\pi}{3}\right) & \cos\left(\theta + \frac{2\pi}{3}\right) \\ \sin(\theta) & \sin\left(\theta - \frac{2\pi}{3}\right) & \sin\left(\theta + \frac{2\pi}{3}\right) \\ \frac{1}{2} & \frac{1}{2} & \frac{1}{2} \end{bmatrix} \tag{A.2}$$

$$T^{-1}(\theta) = \frac{2}{3}\begin{bmatrix} \cos(\theta) & \sin(\theta) & 1 \\ \cos\left(\theta - \frac{2\pi}{3}\right) & \sin\left(\theta - \frac{2\pi}{3}\right) & 1 \\ \cos\left(\theta + \frac{2\pi}{3}\right) & \sin\left(\theta + \frac{2\pi}{3}\right) & 1 \end{bmatrix} \quad \text{(A.3)}$$

However, only choosing the right θ angle, constants values are obtained. This angle corresponds to the electrical voltage angle.

Using the Instantaneous Power Theory for balanced systems [28][29] in the $dq0$ frame, previously replacing θ for the electrical angle $\theta = wt + \varphi_0$ and transforming abc electrical quantities to $dq0$ using Park Transformation for both voltages and currents and defining voltage and current phasors as $\sqrt{2}\underline{V}^{qd} = v_q - jv_d$ and $\sqrt{2}\underline{I}^{qd} = i_q - ji_d$, the apparent power expression in $dq0$ can be deduced from the three phase apparent power expression in abc as (A.4).

$$\underline{S} = P + jQ = 3\underline{V}^{qd}\underline{I}^{qd*} = 3\left(\frac{v_q - jv_d}{\sqrt{2}}\right)\left(\frac{i_q - ji_d}{\sqrt{2}}\right) \quad \text{(A.4)}$$

Rearranging expression (A.4), active and reactive power can be expressed as (A.5) and (A.6) respectively.

$$P = \frac{3}{2}\left(v_q i_q + v_d i_d\right) \quad \text{(A.5)}$$

$$Q = \frac{3}{2}\left(v_q i_d - v_d i_q\right) \quad \text{(A.6)}$$